



A tropospheric ozone maximum over the equatorial Southern Indian Ocean

L. Zhang^{1,2}, Q. B. Li^{1,2}, L. T. Murray³, M. Luo⁴, H. Liu⁵, J. H. Jiang⁴, Y. Mao^{1,2}, D. Chen^{1,2}, M. Gao^{1,2}, and N. Livesey⁴

¹Department of Atmospheric and Oceanic Sciences, University of California, Los Angeles, CA, USA

²Joint Institute for Regional Earth System Science and Engineering, University of California, Los Angeles, CA, USA

³School of Engineering and Applied Sciences, Harvard University, Cambridge, MA, USA

⁴Jet Propulsion Laboratory, California Institute of Technology, CA, USA

⁵National Institute of Aerospace, Hampton, VA, USA

Correspondence to: Q. B. Li (qli@atmos.ucla.edu)

Received: 13 December 2011 – Published in Atmos. Chem. Phys. Discuss.: 20 January 2012

Revised: 27 April 2012 – Accepted: 2 May 2012 – Published: 14 May 2012

Abstract. We examine the distribution of tropical tropospheric ozone (O_3) from the Microwave Limb Sounder (MLS) and the Tropospheric Emission Spectrometer (TES) by using a global three-dimensional model of tropospheric chemistry (GEOS-Chem). MLS and TES observations of tropospheric O_3 during 2005 to 2009 reveal a distinct, persistent O_3 maximum, both in mixing ratio and tropospheric column, in May over the Equatorial Southern Indian Ocean (ESIO). The maximum is most pronounced in 2006 and 2008 and less evident in the other three years. This feature is also consistent with the total column O_3 observations from the Ozone Mapping Instrument (OMI) and the Atmospheric Infrared Sounder (AIRS). Model results reproduce the observed May O_3 maximum and the associated interannual variability. The origin of the maximum reflects a complex interplay of chemical and dynamic factors. The O_3 maximum is dominated by the O_3 production driven by lightning nitrogen oxides (NO_x) emissions, which accounts for 62 % of the tropospheric column O_3 in May 2006. We find the contribution from biomass burning, soil, anthropogenic and biogenic sources to the O_3 maximum are rather small. The O_3 productions in the lightning outflow from Central Africa and South America both peak in May and are directly responsible for the O_3 maximum over the western ESIO. The lightning outflow from Equatorial Asia dominates over the eastern ESIO. The interannual variability of the O_3 maximum is driven largely by the anomalous anti-cyclones over the southern Indian Ocean in May 2006 and 2008. The lightning outflow from Central

Africa and South America is effectively entrained by the anti-cyclones followed by northward transport to the ESIO.

1 Introduction

Ozone (O_3) in the tropical upper troposphere is an effective greenhouse gas (Lacis et al., 1990). Ozone is also an important tropospheric oxidant and modulates the oxidizing power of the troposphere through photolysis in the presence of water vapor that generates hydroxyl radical (OH), the main atmospheric oxidant (Levy, 1971; Logan et al., 1981). Production of tropical tropospheric O_3 is driven by nitrogen oxides ($NO_x = NO + NO_2$) emitted from primarily lightning (e.g., Sauvage et al., 2007; Ziemke et al., 2009) and biomass burning (e.g., Fishman et al., 1990; Jacob et al., 1996; Thompson et al., 2001; Logan et al., 2008). Large-scale dynamics is another prominent factor in controlling tropical tropospheric O_3 distributions (e.g., Chandra et al., 2009; Zhang et al., 2011; Oman et al., 2011, and references therein).

The present study is motivated by an observed tropospheric O_3 maximum in May over the southern tropical Indian Ocean from observations by the Microwave Limb Sounder (MLS), the Tropospheric Emission Spectrometer (TES), the Ozone Mapping Instrument (OMI) aboard the Aura satellite, and the Atmospheric Infrared Sounder (AIRS) aboard Aqua (detailed discussions in Sect. 4). Such an O_3 maximum was indicated in previous observations (e.g.,

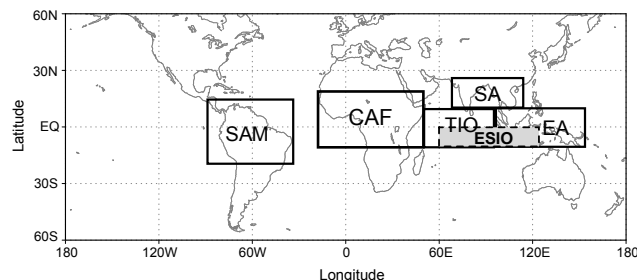


Fig. 1. The Equatorial Southern Indian Ocean (ESIO, 10° S-equator, 60° E– 125° E; shaded area) and five tropical lightning regions: the tropical Indian Ocean (TIO: 10° S– 10° N, 40° E– 95° E), South Asia (SA: 10° N– 30° N, 70° E– 110° E), Equatorial Asia (EA: 10° S– 10° N, 95° E– 150° E), Central Africa (CA: 10° S– 20° N, 20° W– 40° E) and South America (SAM: 20° S– 15° N, 85° W– 35° W).

Komala et al., 1996; Ziemke et al., 2009). We investigate here the origin of this O_3 maximum and its interannual variability by interpreting the satellite observations using a global three-dimensional (3-D) chemical transport model (CTM). We intend to delineate the relative influence of biomass burning, lightning, and dynamics in controlling the O_3 maximum. Much of our analysis focuses on the Equatorial Southern Indian Ocean (10° S-equator (EQ) latitudes, 60° E– 125° E longitudes), referred to hereafter as ESIO (the shaded rectangle in Fig. 1).

We give a brief description of the observations in Sect. 2. Section 3 describes the GEOS-Chem model and simulations. Seasonal variations of tropospheric O_3 in 2006 over the ESIO are discussed in Sect. 4. The lightning impact on tropospheric O_3 over the region is examined in Sect. 5. Section 6 investigates the interannual variability of the tropospheric O_3 enhancements over the ESIO. The results and discussion are summarized in Sect. 7.

2 Observations

2.1 MLS O_3

The Microwave Limb Sounder (MLS) (Waters et al., 2006) aboard the EOS Aura spacecraft (Schoeberl et al., 2006) has been measuring atmospheric parameters since August 2004. MLS uses microwave limb sounding to measure temperature and chemical constituents, including CO, O_3 , water vapor, and cloud ice water content in the upper troposphere and lower stratosphere. MLS measurements in the upper troposphere are generally not degraded by the presence of clouds and aerosols because the typical cloud and aerosol particle sizes are generally much smaller than the measurement wavelengths. MLS measures \sim 3500 vertical profiles per day along a sun-synchronous polar orbit, with an equator-crossing time of \sim 13:45 local time. The data are produced

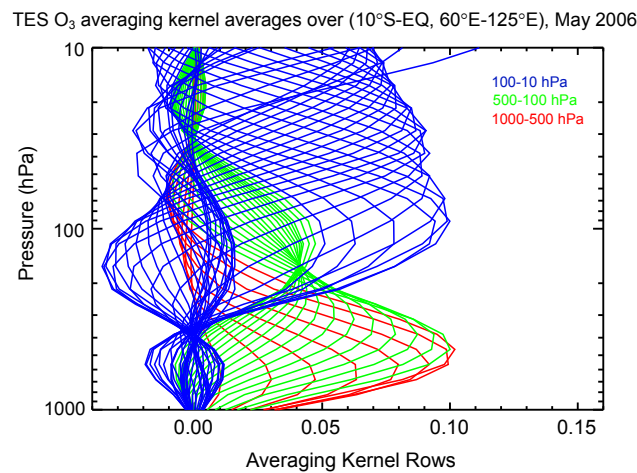


Fig. 2. TES O_3 averaging kernel (between 1000 and 10 hPa), averaged for May 2006 over the Equatorial Southern Indian Ocean (see Fig. 1).

on pressure surfaces from 316 to 0.1 hPa. MLS data has a vertical resolution of \sim 3–4 km and horizontal resolutions of \sim 7 km across-track and \sim 200–300 km along-track (Livesey et al., 2006). We use here O_3 from MLS Version 3.3 (v3.3) Level 2 data (Livesey et al., 2011). Livesey et al. (2008) reported the validation of an earlier version of MLS O_3 (v2.2). The estimated accuracies of MLS v2.2 O_3 are \sim 20 ppbv (+20 %) at 215 hPa and 40 ppbv (+5 %) at 147 hPa. The systematic errors of MLS v3.3 O_3 are consistent with those of v2.2 (Livesey et al., 2011). Our analysis focuses on the observations at 147 and 215 hPa in the upper troposphere. For the present study, the Level 2 MLS data are averaged onto 2° latitude \times 5° longitude grids for every five days as well as monthly from 2005 to 2009. The precision of the O_3 retrieval in the Level 2 data is 5–100 % from 261 to 150 hPa for single measurement (Livesey et al., 2011). The averaged precisions are up to \sim 8 % for the 5-day averages and \sim 4 % for the monthly averages over the ESIO.

2.2 TES O_3

The Tropospheric Emission Spectrometer (TES) is an infrared, high-resolution, Fourier Transform spectrometer covering the spectral range between 3.3 and 15.4 μ m (Beer et al., 2001; Beer, 2006). It was launched on board Aura (Schoeberl et al., 2006) in July 2004 in a sun-synchronous polar orbit. TES provides global vertically resolved measurements of tropospheric O_3 , CO and other atmospheric constituents. TES retrievals have been previously described by Bowman et al. (2006) and Kulawik et al. (2006). For the O_3 retrieval, the prior information is derived from a global model simulation using the Model for OZone And Related chemical Tracers (MOZART, v2) (Horowitz et al., 2003; Brasseur et al., 1998). We use data from TES global surveys, with 16 orbits per global survey, over a time period of 26 h (Osterman et

al., 2008). The nadir O₃ vertical profiles are spaced \sim 182 km apart along the orbit track and have a footprint of 5 km by 8 km (Beer et al., 2001). Under clear sky the vertical resolution of TES O₃ profile retrievals is typically 6 km in the tropics (Jourdain et al., 2007). The TES averaging kernel shows the pressure levels where the retrieval is sensitive to and loosely indicates the vertical resolution of the retrieved profile (Bowman et al., 2006; Worden et al., 2007). Typical TES averaging kernels for O₃ are shown in Worden et al. (2007), Osterman et al. (2008) and Shim et al. (2009). As an illustration, Fig. 2 shows a TES averaging kernel for profiles averaged in May 2006 over the ESIO. The averaged degree of freedom for signal (DOFs) is 1.5 in the troposphere between 1000–100 hPa, suggesting that there are more than one pieces of information in the retrieval and that the profile can be interpreted as distinguishing the upper troposphere versus the middle and lower troposphere.

TES Level 3 gridded data are the species profile interpolated (daily) or averaged (monthly) into uniform longitude-latitude grid from Level 2 data. The precision of a TES O₃ profile is 5%–10% in the troposphere. The monthly averaged a few hundreds of O₃ profiles would reduce the precision to less than 1% over the ESIO, much smaller than the variability in O₃ field in the region. Here we use Version 3 (v3) Level 3 O₃ data (Osterman et al., 2008), including mixing ratio, TCO, and total column O₃ data from 2005 to 2009, monthly averaged at 2° (latitude) \times 4° (longitude) grids. The TES column values (e.g., TCO) were computed by integrating the retrieved profile up to the tropopause pressure as provided in the GEOS-4 meteorological fields (Bloom et al., 2005; Osterman et al., 2008) (see Sect. 3 for more details on the GEOS-4 data). Validation of TES tropospheric O₃ retrievals against ozonesonde and lidar measurements shows a positive bias of \sim 3–10 ppbv (Nassar et al., 2008). The bias of TES TCOs is known to be high by \sim 4 DU in comparison with ozonesonde data (Osterman et al., 2008).

2.3 OMI and AIRS total column O₃

The Ozone Monitoring Instrument (OMI) aboard Aura is a nadir-viewing, wide-swath hyper-spectral imaging spectrometer that provides daily global coverage with high spatial and spectral resolutions (Levelt et al., 2006b). It detects backscattered solar radiance in the ultraviolet-visible wavelengths (0.27 to 0.5 μ m) to measure column O₃ and other trace constituents and aerosols (Levelt et al., 2006a). OMI data has a spatial resolution of 13 \times 24 km² at nadir. Here we use the Level 3 Version 003 (V003) of daily OMI-TOMS (OMTO3) total column O₃ binned onto a 1° (latitude) \times 1° (longitude) grid from 2005 to 2009, which are derived from the TOMS (version 8) algorithm. The accuracy and precision of the OMTO3 total column O₃ data is similar to the legacy Total Ozone Mapping Spectrometer (TOMS) data started in 1978, except over cloudy areas where OMTO3 data are more accurate than that of the TOMS (see http://toms.gsfc.nasa.gov/omi/OMTO3_README_v8_5.pdf).

Based on experience with TOMS, the total O₃ data provided in OMTO3 should have a root-mean squared error of 1–2%, depending on solar zenith angle, aerosol amount, and cloud cover. Validation of the OMI total column O₃ against ground-based observations by Brewer/Dobson spectrophotometer instruments shows generally a better than 1% agreement (Balis et al., 2007; McPeters et al., 2008).

The Atmospheric Infrared Sounder (AIRS) (Aumann et al., 2003) is a high spectral resolution infrared sounder flown aboard the Aqua spacecraft (Parkinson, 2003) and has been operational since September 2002. Aqua is in a sun-synchronous polar orbit, with an equatorial crossing of \sim 13:30 local time, covering the earth twice a day. Validation of AIRS total column O₃ against ground-based Brewer/Dobson measurements shows a bias of less than 4% and a root-mean-square error of approximately 8% (Divakarla et al., 2008). We use AIRS Version 5 (V5) Level 3 monthly total column O₃ binned onto a 1° (latitude) \times 1° (longitude) grid from 2005 to 2009.

3 GEOS-Chem model description and simulations

GEOS-Chem is a global 3-D CTM driven by assimilated meteorological observations from the Goddard Earth Observing System (GEOS) of the NASA Global Modeling and Assimilation Office (GMAO) (Bey et al., 2001). We use GEOS-Chem version 8-01-04 (<http://acmg.seas.harvard.edu/geos/>) driven by GEOS-4 and GEOS-5 meteorological fields with 6-h temporal resolution (3-h for surface variables and mixing depths), 2° (latitude) \times 2.5° (longitude) horizontal resolution, and 30 (GEOS-4) or 47 (GEOS-5) vertical layers between the surface and 0.01 hPa. The GEOS-Chem model includes a detailed description of tropospheric O₃-NO_x-hydrocarbon chemistry coupled with aerosol chemistry (Bey et al., 2001). Gas phase chemical reaction rates and photolysis cross sections are taken from Sander et al. (2000). Photolysis frequencies are computed using the Fast-J algorithm (Wild et al., 2000). The cross-tropopause O₃ flux is specified with the “synthetic ozone” (Synoz) method (McLinden et al., 2000) as implemented by Bey et al. (2001). Synoz includes a passive, ozone-like tracer released into the stratosphere at a rate that results in a prescribed cross-tropopause O₃ flux (McLinden et al., 2000), thereby ensuring that downward ozone flux from the stratosphere is not overestimated. The cross-tropopause NO_y flux is calculated from N₂O oxidation in the model stratosphere (Bey et al., 2001). The global net cross-tropopause fluxes of O₃ and NO_y are 495 Tg O₃/yr and 0.5 Tg N/yr, respectively in the model (Hudman et al., 2007). The GEOS-Chem model also includes a linearized ozone (“Linoz”) parameterization scheme based on the work by McLinden et al. (2000) to represent the ozone in the stratosphere, in which the ozone vertical profiles across the tropopause are relaxed back toward climatological profiles.

The Synoz scheme may not correctly capture the variability in the magnitude of the local stratospheric ozone fluxes, but, as Liu et al. (2009) pointed out, that the mean differences in ozone abundances in the tropical middle troposphere simulated with the two schemes are within 3 %.

Tracer advection is computed every 15 min with a flux-form semi-Lagrangian method (Lin and Rood, 1996). Tracer moist convection is computed using the GEOS convective, entrainment, and detrainment mass fluxes as described by Allen et al. (1996a, b). The deep convection scheme of GEOS-4 is based on Zhang and McFarlane (1995), and the shallow convection treatment follows Hack (1994). GEOS-5 convection is parameterized using the relaxed Arakawa-Schubert scheme (Moorthi and Suarez, 1992).

Emissions of lightning NO_x in GEOS-Chem are computed locally in deep convection events following the scheme of Price and Rind (1992) that relates flash rates to convective cloud top heights. The NO_x emissions are vertically distributed following the profile from Pickering et al. (1998) where 55–75 % of the emissions are above 8 km. Implementation of the lightning source in GEOS-Chem is as described by Wang et al. (1998) with some recent updates (Hudman et al., 2007; Sauvage et al., 2007; Nassar et al., 2009; Jourdain et al., 2010; Murray et al., 2012). The model also includes two alternative lightning schemes that link flash rates to either convective precipitation or upward convective mass flux, following Allen and Pickering (2002). The lightning modules as implemented in GEOS-Chem based on the aforementioned three schemes are hereafter referred to as CTH, PREC, and MFLUX, respectively. To improve the spatial distribution of lightning in the model, the spatial distribution of lightning is scaled to reproduce seasonal mean lightning flash rates to match the climatological satellite observations of lightning flashes from the Optical Transient Detector and Lightning Imaging Sensor (OTD/LIS) High Resolution Monthly Climatology (HRMC) v2.2 product (Christian et al., 2003). Globally the lightning NO_x source is scaled to 6 Tg N yr⁻¹ (Martin et al., 2007; Hudman et al., 2007; Sauvage et al., 2007).

Lightning flash rates in global atmospheric models are usually parameterized from functions of proxies of deep convection, enabling the linking of lightning NO_x emissions with the concurrent convective transport of surface precursors. We test here those based on convective cloud top heights (CTH) (Price and Rind, 1992, 1993, 1994), upward convective mass flux (MFLUX) (Allen et al., 2000), and total convective precipitation (PREC) (Allen and Pickering, 2002) using 6-h mean archived meteorology from the Goddard Earth Observing System Data Assimilation System (GEOS DAS) version 5.1.0. Once the flash rate is determined for a grid box, a NO_x per flash yield is applied, and the NO_x emissions are vertically distributed throughout the column following the probability distribution functions of Pickering et al. (1998). The CTH parameterization was originally implemented by Wang et al. (1998) and MFLUX and PREC by

Murray et al. (2012). Each parameterization shows little skill in matching the spatial and seasonal distribution of flash rates observed in the long-term mean Lightning Imaging Sensor and Optical Transient Detector (LIS/OTD) High Resolution Monthly Climatology (HRMC) v2.2 satellite product, and therefore techniques have been variously implemented to constrain the flash rates derived from the GEOS met fields (e.g., Sauvage et al., 2007; Jourdain et al., 2010; Allen et al., 2010; Murray et al., 2012). We also use here an optional “local redistribution” as implemented by Murray et al. (2012). It applies a local seasonal rescaling factor based on space-based observations of lightning flash counts from the multi-year seasonally varying climatological lightning flashes from HRMC product to constrain GEOS-Chem lightning flashes (Sauvage et al., 2007; Murray et al., 2012). Due to the lack of GEOS-5 meteorological fields during the observation period of the HRMC product (May 1995 through December 2005), we determine the constraint using the long-term monthly mean from all available months of GEOS v5.1.0 meteorology (January 2004 through August 2008).

Biomass burning emissions are long known to be a key factor influencing tropical tropospheric O₃ (Fishman et al., 1990; Jacob et al., 1996; Thompson et al., 1996). Biomass burning emissions in the present study are from GFED v2 that resolves the interannual variability of biomass burning emissions (van der Werf et al., 2006; Randerson et al., 2006). GFED v2 is derived using satellite observations including active fire counts and burned areas in conjunction with the Carnegie-Ames-Stanford-Approach (CASA) biogeochemical model. Carbon emissions are calculated as the product of burned area, fuel load and combustion completeness. Burned area is derived using the active fire and 500-m burned area datasets from the Moderate Resolution Imaging Spectroradiometer (MODIS) as described by Giglio et al. (2006). The original GFED v2 inventory has a spatial resolution of 1° (latitude) × 1° (longitude) and a monthly temporal resolution. The emissions are re-sampled to 2° (latitude) × 2.5° (longitude) grids for use in our GEOS-Chem simulations. Forest fires typically last from several days to weeks as seen in MODIS active fires (Giglio et al., 2003). Therefore, we re-sampled GFED v2 monthly emissions to an 8-day time step according to MODIS 8-day active fire counts (Chen et al., 2009). The GFED v2 8-day emissions are used for the model simulations presented here unless stated otherwise.

The fossil fuel emissions are from the Emission Database for Global Atmospheric Research (EDGAR) inventory for NO_x, CO, and SO₂ (Olivier et al., 2001) and from the Global Emission Inventory Activity (GEIA) for other chemical compounds (Benkovitz et al., 1996) with additional updates as described by Hudman et al. (2007). Asian anthropogenic emissions are updated with the estimates from Zhang et al. (2009). Biofuel emissions are from Yevich and Logan (2003). The biogenic VOCs emissions are based on the

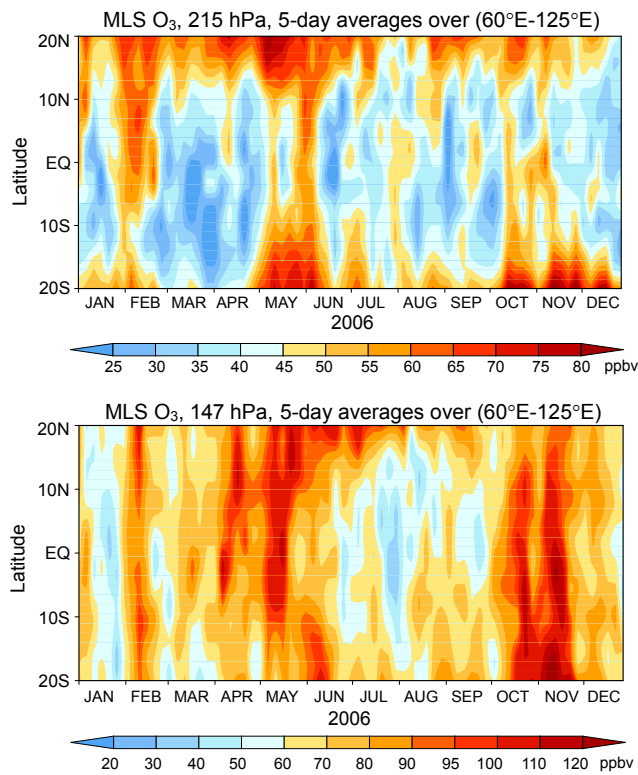


Fig. 3. MLS observed upper tropospheric O₃ at (top panel) 215 hPa and (bottom panel) 147 hPa over 20° S–20° N for 2006. Values are 5-day averages over the 60° E–125° E longitudes.

Model of Emissions of Gases and Aerosols from Nature (MEGAN) inventory (Guenther et al., 2006).

We conducted model simulations from 2005 to 2009 driven by either GEOS-4 or GEOS-5 meteorological data. We calculated the TCO by integrating the simulated O₃ vertical profiles up to the tropopause as provided in the GEOS meteorological fields. The tropopause in GEOS is defined as the pressure where the function $aT(p) - \log_{10} p$ ($\alpha = 0.03$, T is temperature and p is pressure) reaches its first minimum above the surface, and it varies at each dynamic time step of the model (Rienecker, 2008). The tropopause pressures in GEOS-4 and GEOS-5 are approximately the same to each other in tropics (Zhang et al., 2011). In the comparisons between observations and model results, we applied the same spatial and temporal averaging. Our analysis focuses on the results for 2006. For the comparisons of model results based on different meteorological fields and lighting parameterizations, the details for these simulations are summarized in Table 1. Justifications for these simulations are provided in Sect. 5.

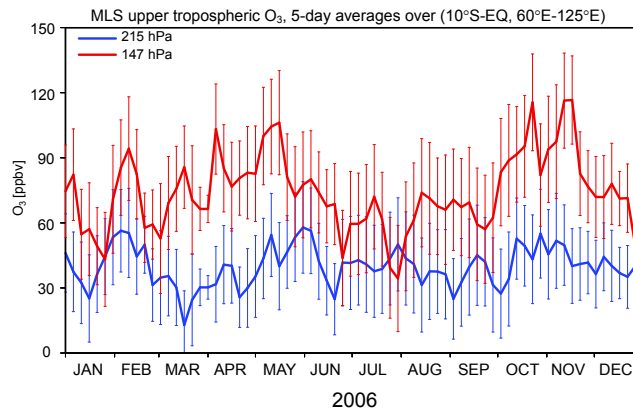


Fig. 4. MLS O₃ at 147 (red line) and 215 hPa (blue line), averaged over the Equatorial Southern Indian Ocean (see Fig. 1) for 2006. Values are 5-day averages. Vertical bars indicate standard deviations of the measurements.

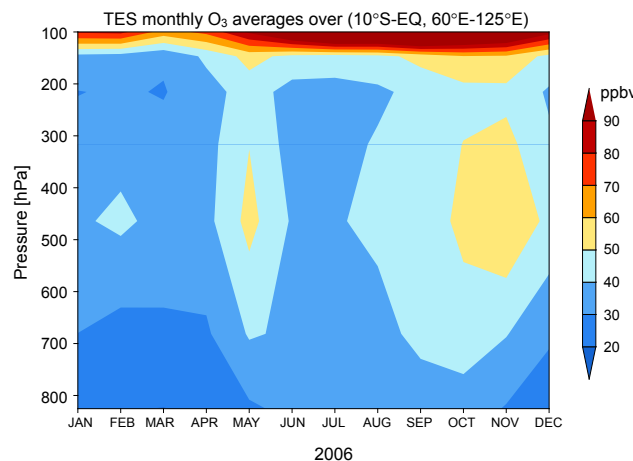


Fig. 5. TES tropospheric O₃ vertical distribution averaged over the Equatorial Southern Indian Ocean (see Fig. 1). Values are monthly means for 2006.

4 Seasonal variation of tropospheric O₃ over the ESIO

4.1 MLS upper tropospheric O₃

Figure 3 shows MLS O₃ concentrations at 20° S–20° N, averaged between 60° E and 125° E for 2006. The values are 5-day averages. South of the equator at 215 hPa the O₃ concentrations show a broad maximum during May and early June when the concentrations are higher by 20 to 30 ppbv relative to those during March and April. This maximum is the focus of the present study. There is a secondary peak during late June and early July with maximum concentrations confined to the region between 10° S and 20° S latitudes. Similar yet considerably enhancements are also evident at 147 hPa during May and June and larger than those at 215 hPa. The O₃ enhancements during October and November, seen at both 215 and 147 hPa, are largely because of the extensive fires

Table 1. Description of model simulations.

Experiment	Year	Meteorological data	Lightning parameterization
A1	2006	GEOS-4	Convective cloud-top-height
A2	2006	GEOS-4	Convective cloud-top-height with local redistribution
A3	2006	GEOS-4	Convective mass flux
A4	2006	GEOS-4	Convective precipitation
B1	2006	GEOS-5	Convective cloud-top-height
B2	2006	GEOS-5	Convective cloud-top-height with local redistribution

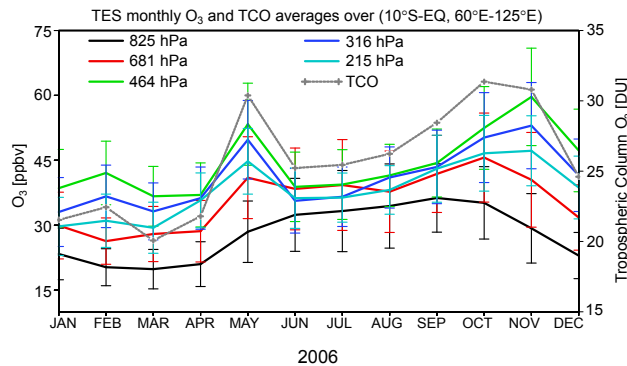


Fig. 6. TES tropospheric O₃ and tropospheric column O₃ (TCO) over the Equatorial Southern Indian Ocean (see Fig. 1). Values are monthly means for 2006. Vertical bars indicate standard deviations of the measurements.

in Equatorial Asia (mostly in southern Borneo and Sumatra) that lasted from September through November 2006 and the dynamic changes pertained to the 2006 El Niño (Zhang et al., 2011, and references therein). Figure 4 shows time series of MLS O₃ at 215 and 147 hPa averaged over the entire ESIO domain (Fig. 1) for 2006. Again, broad enhancements of O₃ are evident during May–June with maximum O₃ concentrations exceeding 55 ppbv at 215 hPa and 100 ppbv at 147 hPa.

4.2 TES middle and upper tropospheric O₃

TES tropospheric O₃ also shows a distinct maximum in May 2006 over the ESIO, and the enhancement extends throughout the middle and upper troposphere with peak values above 50 ppbv (Fig. 5). The pronounced and broad O₃ enhancements in the middle and upper troposphere during September through December are largely because of the 2006 Indonesian fires in Equatorial Asia (Logan et al., 2008; Nassar et al., 2009; Zhang et al., 2011). Figure 6 shows TES monthly tropospheric O₃ and TCO over the ESIO for 2006. Both tropospheric O₃ and TCO show seasonal maxima in May and during September through November. The largest O₃ enhancements in May are in the middle to upper troposphere, with peak mixing ratios over 50 ppbv at 464 hPa. The peak values of TES TCO are over 30 DU in May and in October and November.

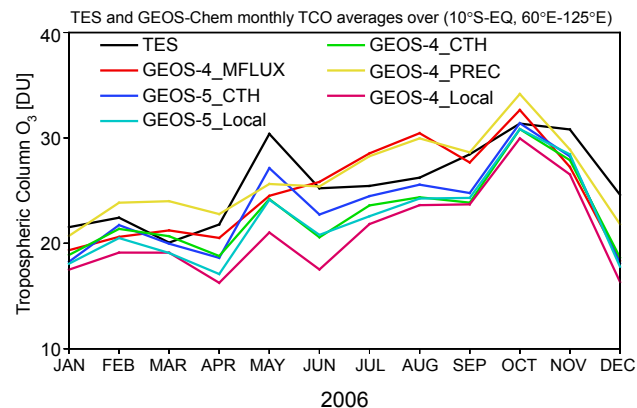


Fig. 7. TES retrieved and GEOS-Chem simulated monthly mean tropospheric column O₃ (TCO) for 2006 over the Equatorial Southern Indian Ocean (see Fig. 1). Model results from simulations driven by GEOS-4 and by GEOS-5 reanalysis data and with different lightning parameterizations are shown. See text for more detail.

5 Lightning impact on tropospheric O₃ over the ESIO

5.1 Sensitivity to lightning parameterization

GEOS-Chem simulations of tropospheric O₃ have significant dependence on the differences of the lightning parameterizations and the meteorological data used. To examine this sensitivity, we conducted six sensitivity simulations (summarized in Table 1), driven by GEOS-4 or GEOS-5 meteorological data, using the different lightning parameterizations (see Sect. 3). Model TCO averaged over the ESIO are compared against TES data and shown in Fig. 7. For direct comparison to the observations, we calculated monthly mean TCO averages over EISO from model results and TES observations. In general, when comparing TES profiles with other measurements, it is essential to take into account the different sensitivities of the instruments by applying TES averaging kernels (Luo et al., 2007; Worden et al., 2007). However, comparing columns rather than individual profiles significantly reduces the error due to averaging over pressure ranges larger than the TES vertical resolution, 1.5 % for O₃ columns averages as compared to 16.5 % for the average profile error between the surface and 35 km altitude (Osterman et al., 2008). As such, we did not convolve TES averaging kernels with

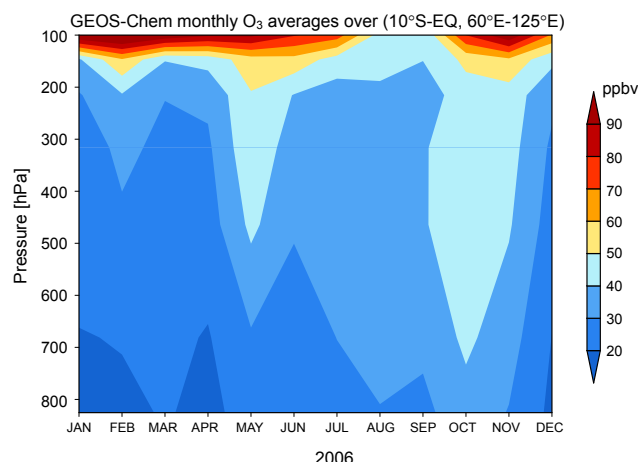


Fig. 8. GEOS-Chem simulated tropospheric O₃ vertical distribution averaged over the Equatorial Southern Indian Ocean (see Fig. 1). Values are monthly means for 2006.

GEOS-Chem simulated O₃ profiles when calculating model TCOs.

Model simulations A1–A4 were driven by GEOS-4 meteorological data. A1 and A2 used the same CTH lightning parameterization, but A2 used the local redistribution of lightning flash rates based on LIS/OTD observations (Sect. 3) while A1 did not. A3 and A4 used the MFLUX and the PREC lightning parameterizations, respectively, and neither included the local redistribution factors. Given the way lightning is linked to deep convection in the model, the different deep convection parameterizations used in GEOS-4 and GEOS-5 will also lead to differences in the lightning NO_x emissions in the model. To examine this sensitivity, we conducted two additional simulations driven by GEOS-5 meteorological data, B1 and B2. Other than the GEOS-5 meteorological data used, B1 and B2 mirror A1 and A2, respectively.

Figure 7 shows that B1, driven by GEOS-5 data and with the CTH lightning parameterization, best captures the seasonal variation of TES TCO, including the enhancement in May 2006. Model results are consistently lower than the observations by up to 4 DU for all months. That is not a systematic bias necessarily because TES TCOs are known to be biased high by ~4 DU in comparison with ozonesonde data (Osterman et al., 2008). A1, driven by GEOS-4 data and with the CTH lightning parameterization, significantly underestimates the TCO throughout the year. A3 and A4, driven by GEOS-4 data and with the MFLUX and the PREC lightning parameterizations, show no apparent relative enhancements of TCO in May 2006. Neither reproduces the observed TCO seasonal variation. A2 and B2, using a local redistribution factor of lightning flash rates based on LIS/OTD data, show no obvious improvements to A1 and B1. In fact, both A2 and B2 show substantially lower TCOs in comparison with not only A1 and B1, respectively, but also TES observations. Therefore, we choose B1 set up as our standard simulation:

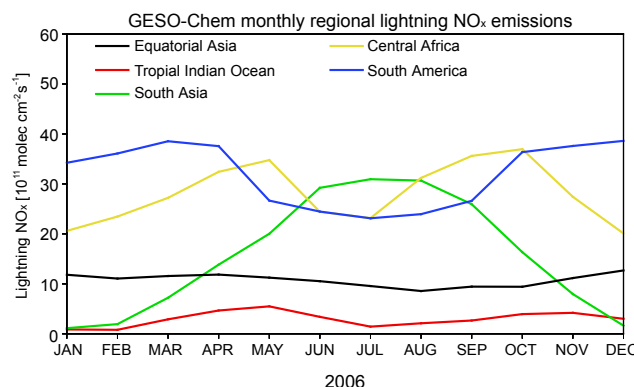


Fig. 9. GEOS-Chem simulated lightning NO_x emissions over Equatorial Asia (black line), Central Africa (yellow line), South America (blue line), South Asia, and the tropical Indian Ocean (red line). Values are monthly means for 2006. See Fig. 1 for domain definitions.

GEOS-Chem simulation driven by GEOS-5 meteorological data using the CTH lightning parameterization without local redistribution factor for flash rates. And all the following analyses are based on the B1 set up.

Figure 8 shows the simulated tropospheric O₃ in May 2006 over the EISO by using the above set up. Model reproduces the two enhancements (May and October) extend throughout the middle and upper troposphere as the TES observation, though it underestimates the maximum O₃ concentration in the middle troposphere with peak values above 40 ppbv (Fig. 8). The horizontal distributions of tropospheric O₃ and TCO are compared between GEOS-Chem and satellite observations (figures are not shown here). The values of TES and GEOS-Chem TCO is about 15~25 DU in April 2006 over the equatorial areas from 60° E to the eastern Pacific Ocean. The TCO suddenly increases nearly 10 DU in May over the EISO, while decreases from June. GEOS-Chem underestimates about 4~5 DU in May compared to TES observation over the Indonesian regions and equatorial areas of Asia. The simulated upper tropospheric O₃ is lower than that of the MLS in May 2006 over the EISO and surrounding areas.

5.2 Regional lightning NO_x emissions in the tropics

To examine the relative contributions from lightning, we focus our analysis on the following geographical regions (Fig. 1): the tropical Indian Ocean (10° S–10° N, 40° E–95° E), South Asia (10° N–30° N, 70° E–110° E), Equatorial Asia (10° S–10° N, 95° E–150° E), Central Africa (10° S–20° N, 20° W–40° E) and South America (20° S–15° N, 85° W–35° W). Figure 9 shows the seasonal variations of monthly lightning NO_x emissions from the aforementioned five regions. Again, these results are from the standard simulation driven by GEOS-5 meteorological data and with the CTH lightning parameterization (simulation B1).

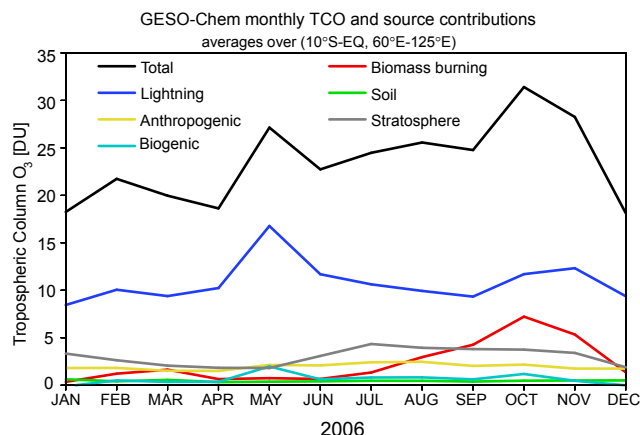


Fig. 10. GEOS-Chem simulated tropospheric column O₃ over the Equatorial Southern Indian Ocean (see Fig. 1). Values are monthly means for 2006. Also shown are tropospheric column O₃ because of NO_x emissions from lightning (blue line), biomass burning (red line), soil (green line), stratospheric downward transport (grey line), anthropogenic sources (yellow line), and biogenic sources (cyan line).

The seasonal variations of lightning NO_x vary considerably among the regions. Lightning NO_x emissions from South Asia show a broad maximum during June–August, the intense phase of the Asian monsoon with abundant convective activities. Central African lightning NO_x emissions are largest first in May and then in September–October. Lightning NO_x emissions from South America show peaks during March through April and then October through December. Equatorial Asia lightning NO_x emissions show little seasonal variation and are at least a factor of two smaller than those from South Asia, Central Africa and South America. Lightning NO_x emissions from the tropical Indian Ocean are smallest among the five regions but peak in May. In May, the largest lightning NO_x emissions are from Central Africa and South America.

5.3 Lightning contribution to tropospheric O₃ over the ESIO

We conducted several sensitivity simulations for 2006 to quantify the relative contributions to the tropical tropospheric O₃ over the ESIO from NO_x emissions from lightning, biomass burning, soil, stratospheric downward flux, anthropogenic activities and biogenic sources by shutting off these sources individually. The difference between these sensitivity simulations and the standard simulation are thus the contributions from the corresponding sources except the stratospheric downward flux. Here the contribution of the stratospheric downward flux is quantified by the tagged O₃ simulation. For tagged O₃ analysis, the Synoz scheme can ensure that the source of O₃ from the stratosphere would not be overestimated (Liu et al., 2009, 2011), since assimilated meteoro-

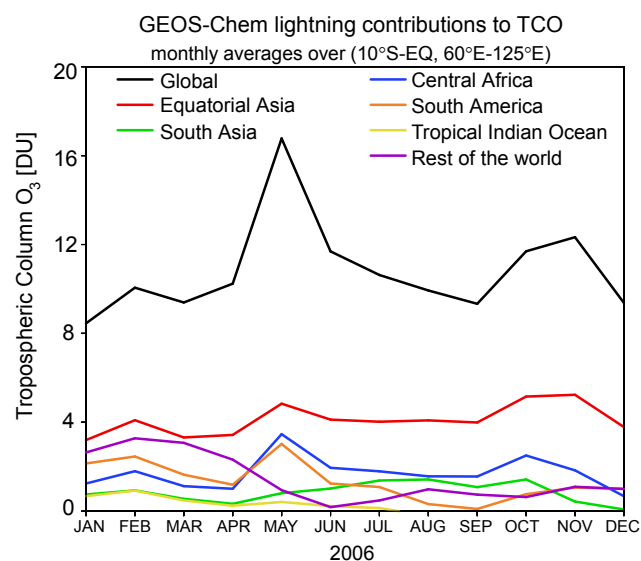


Fig. 11. GEOS-Chem simulated total and lightning tropospheric column O₃ over the Equatorial Southern Indian Ocean (see Fig. 1). Lightning O₃ refers to O₃ produced as a result of lightning NO_x emissions. Values are monthly means for 2006. Tropospheric column O₃ from lightning NO_x emissions over Equatorial Asia, Central Africa, South America, South Asia, and the tropical Indian Ocean (see Fig. 1) are shown.

logical fields produce excessive stratosphere-to troposphere exchange (Weaver et al., 1993; Tan et al., 2004). Therefore, the cross-tropopause flux of O₃ can be matched to observations, which can correctly reproduce the annual global source of stratospheric O₃ (McLinden et al., 2000; Liu et al., 2009). Again, all simulations are driven by GEOS-5 meteorological data and with the CTH lightning parameterization. The resulting contributions, calculated as monthly TCOs averaged over the ESIO, are shown in Fig. 10.

Lightning contribution is ~10 DU on average for much of the year and peaks in May, accounting for more than 60 % of the total TCO with 17 DU, and are directly responsible for the O₃ enhancement in May. Biomass burning has a rather small contribution during January to July. The significant biomass burning impact during September to November is associated with the 2006 fires in Equatorial Asia (Logan et al., 2008; Chandra et al., 2009; Nassar et al., 2009; Zhang et al., 2011). Lightning also makes a significant contribution to the September–November enhancement, as seen in Fig. 10 and was discussed in more detail by Zhang et al. (2011). Without any relative enhancement in May, however, stratospheric downward flux merely provides a background to TCO throughout the year. The contributions from soil and anthropogenic activities are negligibly small (less than 2.5 DU) throughout the year, and none of which peaks in May. Though the contribution from biogenic emission has a peak in May, the contribution is considerably smaller, too.

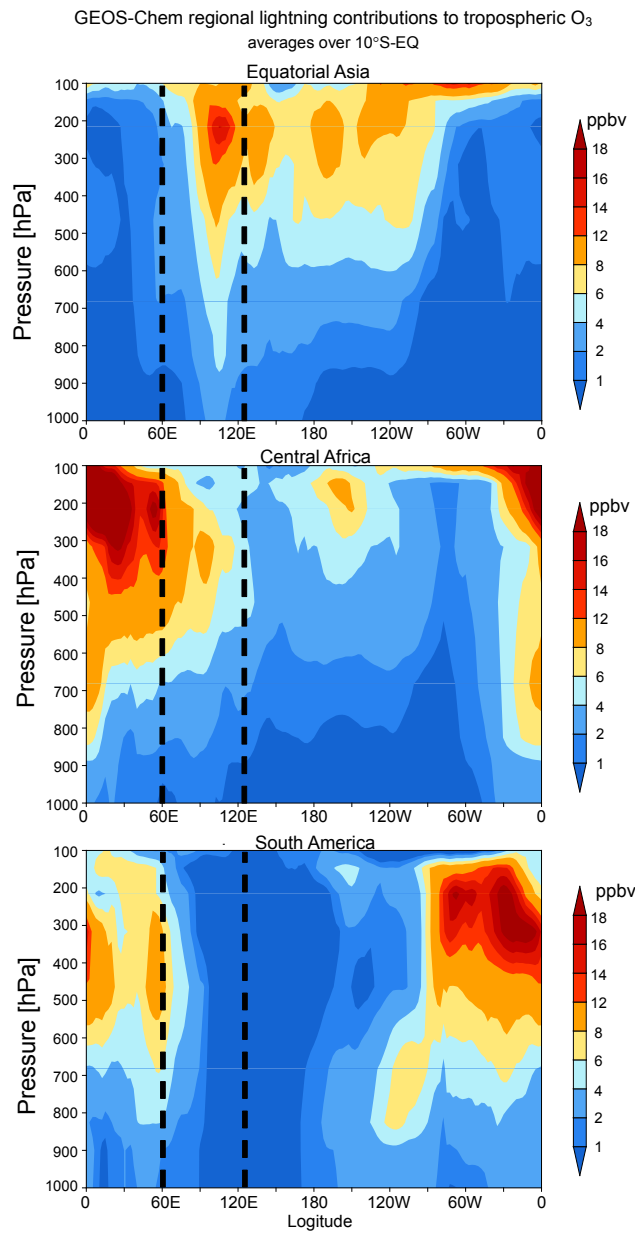


Fig. 12. GEOS-Chem simulated vertical and longitudinal distributions of tropospheric O₃ from Lightning NO_x emissions from (top panel) Equatorial Asia, (middle panel) central Africa, and (bottom panel) South America. Values are monthly means for May 2006, averaged over 10° S to the equator.

Several sensitivity simulations were conducted by turning off the lightning NO_x emission from different sources regions (Fig. 1) to quantify their relative contributions. The difference between these sensitivity simulations and the standard simulation are thus the lightning NO_x contributions from the corresponding sources regions. The relative contributions to the TCO over the ESIO from lightning NO_x emissions from the five regions (Fig. 1) are shown in Fig. 11 and summarized in Table 2. Lightning NO_x emissions from

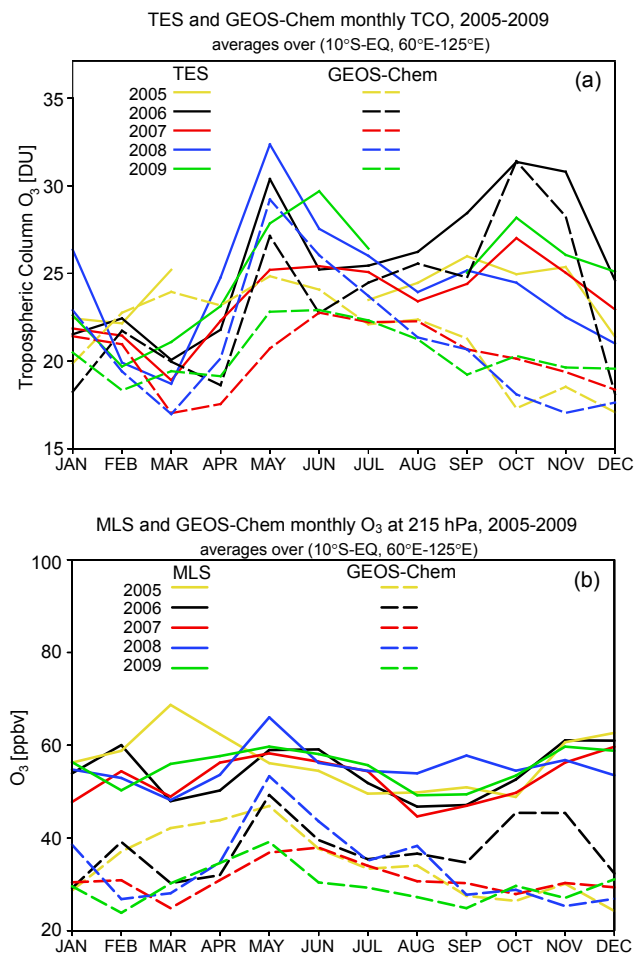


Fig. 13. Observed and simulated tropospheric column O₃ (**a**: TES – solid lines; GEOS-Chem – dashed lines) and 215 hPa O₃ (**b**: MLS – solid lines; GEOS-Chem – dashed lines) over the Equatorial Southern Indian Ocean (see Fig. 1). Values are monthly averages for 2005 to 2009.

Equatorial Asia contribute ~4 to 5 DU to TCO from April to December 2006, with relative enhancements in May (29.2 % of the total lightning TCO, i.e., TCO resulting from lightning NO_x emissions) and October–November. Interestingly and somewhat surprisingly, the contributions to TCO from Central African and South American lightning NO_x emissions both show sharp peaks in May, ~3.5 DU (20.8 % of the total lightning TCO) for Central Africa and 3.0 DU (17.9 % of the total lightning TCO) for South America. We will discuss the lightning outflow from these two regions and its transport to the ESIO in subsequent sections. Figure 11 shows that lightning NO_x emissions from South Asia make relatively small contributions to the TCO enhancement in May (less than 1 DU or 4.8 %) and through much of the year, with a slight uptick during the summer months (~1 to 2 DU). The contribution from lightning NO_x emissions from the tropical Indian Ocean is negligibly small (less than 0.5 DU or 2.4 %) all

year long. Together, lightning NO_x emissions from the aforementioned five regions lead to 75.1 % of the total lightning TCO in May 2006 over the ESIO. Lightning NO_x emissions from the rest of the world contribute 5.4 % (0.9 DU). This contribution is comparable to that from South Asia lightning NO_x emissions in May and much smaller than those from the Equatorial Asia, Central Africa and South America. Without any relative enhancement in May, however, it decreases from April and merely provides a low background. The lightning NO_x emissions from the rest of the world contribute less than the remaining to the five sub-domains reflects not only the nonlinearity of O₃ production but also the transport impacts. In effect, lightning NO_x emissions from Equatorial Asia, Central Africa and South America and subsequent O₃ production determine the O₃ maximum in May 2006. Overall, lightning TCO accounts for 61.8 % of the total TCO over the ESIO in May 2006, of which 18.0 %, 12.9 %, and 11.0 % are because of the lightning NO_x emissions from Equatorial Asia, Central Africa and South America, respectively (Fig. 11 and Table 2).

Figure 12 shows the modeled vertical and longitudinal distributions of monthly average O₃ over 10° S-equator, resulting from the contributions of lightning NO_x emissions from Equatorial Asia, Central Africa and South America in May 2006. The O₃ mixing ratios are averaged over the latitudinal range of EISO (10° S-equator). The two dashed lines indicate the longitudinal range of the ESIO. There is widespread Equatorial Asian lightning O₃ in the middle and upper troposphere over a broad swath between 60° E and 60° W longitudes, with peak O₃ mixing ratios (~18 ppbv) at 150 to 300 hPa over the eastern ESIO (Fig. 12, top panel). These peak O₃ mixing ratios from Equatorial Asian lightning O₃ contribute directly to the O₃ enhancements in the upper tropopause in May (see Figs. 3, 4, 5 and 6). A tongue of Equatorial Asian lightning O₃ extends down to the lower troposphere over the eastern ESIO because of intense deep convective activities in that region. Lightning O₃ from Central Africa makes a significant contribution to O₃ (6 to 12 ppbv) in the middle and upper troposphere over much of the ESIO, with peak values (12 ppbv) at 200 to 500 hPa over the western ESIO (Fig. 12, middle panel). The contribution from South American lightning O₃ (4 to 8 ppbv) is primarily in the middle to upper troposphere over the western ESIO (Fig. 12, bottom panel).

6 Interannual variability of tropospheric O₃ over the ESIO

6.1 Tropospheric O₃ over the ESIO from 2005 to 2009

We investigate in this section the interannual variability of the tropospheric O₃ over the ESIO. For this purpose we examined five years (2005 to 2009) of TES TCO and MLS upper tropospheric O₃ observations (Fig. 13). Relative en-

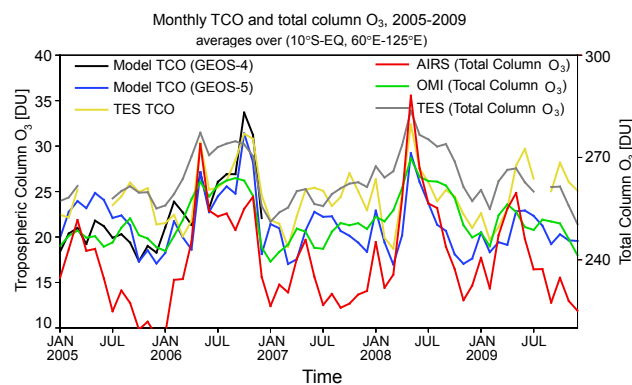


Fig. 14. Monthly mean tropospheric column O₃ from GEOS-Chem (black and blue lines) and TES (yellow line) and total column O₃ from AIRS (red line), OMI (green line) and TES (grey line) over the Equatorial Southern Indian Ocean (see Fig. 1) for 2005 to 2009. Results from model simulations driven by GEOS-4 (black line) and GEOS-5 (blue) reanalysis data are both shown. See text for more detail.

hancements of TCO are seen in May 2006, 2007, 2008 and 2009 (no TES data for April through June 2005) in both TES observations and model results (Fig. 13a). The enhancements are pronounced and largest in May 2006 and 2008 with TCO values over 30 DU. The enhancements in 2007 and 2009 extend from May through July and peak in June. Model results also capture the distinct relative enhancements during October–November 2006 that are related to the 2006 Indonesian fires (Zhang et al., 2011, and references therein) but completely miss those for 2007 and 2009 when model results are vastly lower than the observations in September–December. Overall, model simulated TCOs show seasonal variations that are broadly consistent with the observations for 2006 and 2008. Upper tropospheric O₃ at 215 hPa also show clear relative enhancements in May 2006 and 2008, both in MLS observations and model results (Fig. 13b). The lightning play an important role in contributing to the upper tropospheric O₃ enhancements in May, especially the lightning NO_x emissions from Equatorial Asia (see Fig. 12). Model results are generally lower by 20 ppbv than the observations, but MLS O₃ at 215 hPa is known to have a positive bias of ~20 ppbv (Livesey et al., 2008, 2011). Model results capture the seasonal cycles of O₃ observed by MLS in 2006 but fail to reproduce the enhancements in November and December for other years.

Figure 14 compares GEOS-Chem simulated TCO with TCO from TES and total column O₃ from AIRS, OMI and TES. Model results from two simulations driven by GEOS-4 (2005 to 2006) and by GEOS-5 (2005 to 2009) meteorological data are shown. There are considerable differences among the total column O₃ from the three satellite data sets. The interannual variability of OMI total column O₃ correlates very well with that of TES, but much lower than TES. This has also been pointed out by previous study that TES is higher

Table 2. GEOS-Chem simulated total and lightning tropospheric column O₃ over the Equatorial Southern Indian Ocean (see Fig. 1). Values are monthly averages for May 2006.

Monthly total TCO over ESIO = 27.2 [DU], May 2006					
Total lightning contribution = 16.8 [DU] (61.8 %)					
Regional lightning contribution					
Equatorial Asia	Central Africa	South America	South Asia	Tropical Indian Ocean	Rest of the world
4.9 [DU] (18.0 %)	3.5 [DU] (12.9 %)	3.0 [DU] (11.0 %)	0.8 [DU] (3.0 %)	0.4 [DU] (1.5 %)	0.9 [DU] (3.3 %)
Percentage of total lightning contribution from regional lightning					
29.2 %	20.8 %	17.9 %	4.8 %	2.4 %	5.4 %

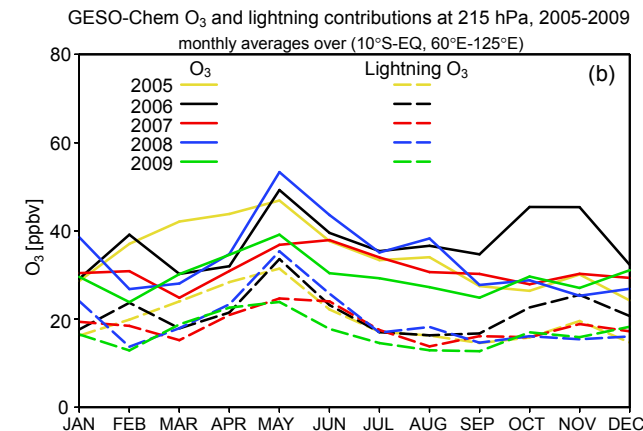
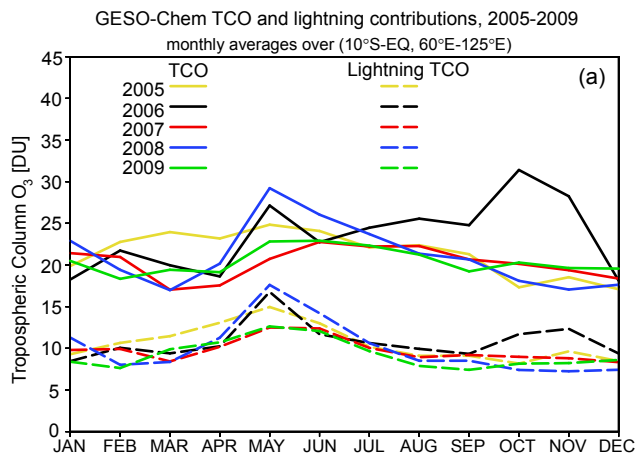


Fig. 15. GEOS-Chem simulated (a) total and lightning tropospheric column O₃ and (b) 215 hPa total and lightning O₃ over the Equatorial Southern Indian Ocean (see Fig. 1). Lightning O₃ refers to O₃ produced as a result of lightning NO_x emissions. Values are monthly means for 2005 to 2009.

than OMI by 10 DU for the total column O₃ (Osterman et al., 2008). Most of the temporal variations of AIRS total column O₃ also follow those of TES and OMI. Other than the

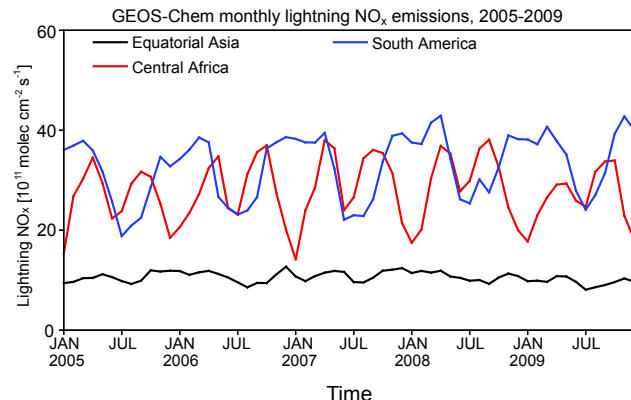


Fig. 16. GEOS-Chem simulated lightning NO_x emissions over Equatorial Asia, Central Africa, and South America (see Fig. 1). Values are monthly means for 2005 to 2009.

enhanced total column O₃ periods, AIRS total column O₃ is much lower than those of TES and OMI during most of the periods. These differences may be due to sampling bias (e.g., AIRS am but TES/OMI pm). Our comparison between GEOS-Chem TCO and the satellite observed total column O₃ is qualitative rather than quantitative, and we focus on the temporal variability of O₃. Robust TCO and total column O₃ enhancements are seen in every May from 2005 to 2009 in both the observations and model results. Again, the observed total column O₃ enhancements are most distinct in May of 2006 and 2008 in AIRS, TES and OMI observations. The large O₃ enhancements during September–November 2006 are associated with the 2006 Indonesian fires (Logan et al., 2008; Chandra et al., 2009; Nassar et al., 2009; Zhang et al., 2011). Model simulations driven by GEOS-5 reanalysis reproduce the observed enhancements and the interannual variability.

6.2 Interannual variability of lightning O₃

We conducted model sensitivity simulations driven by GEOS-5 meteorological data for 2005–2009 to quantify the

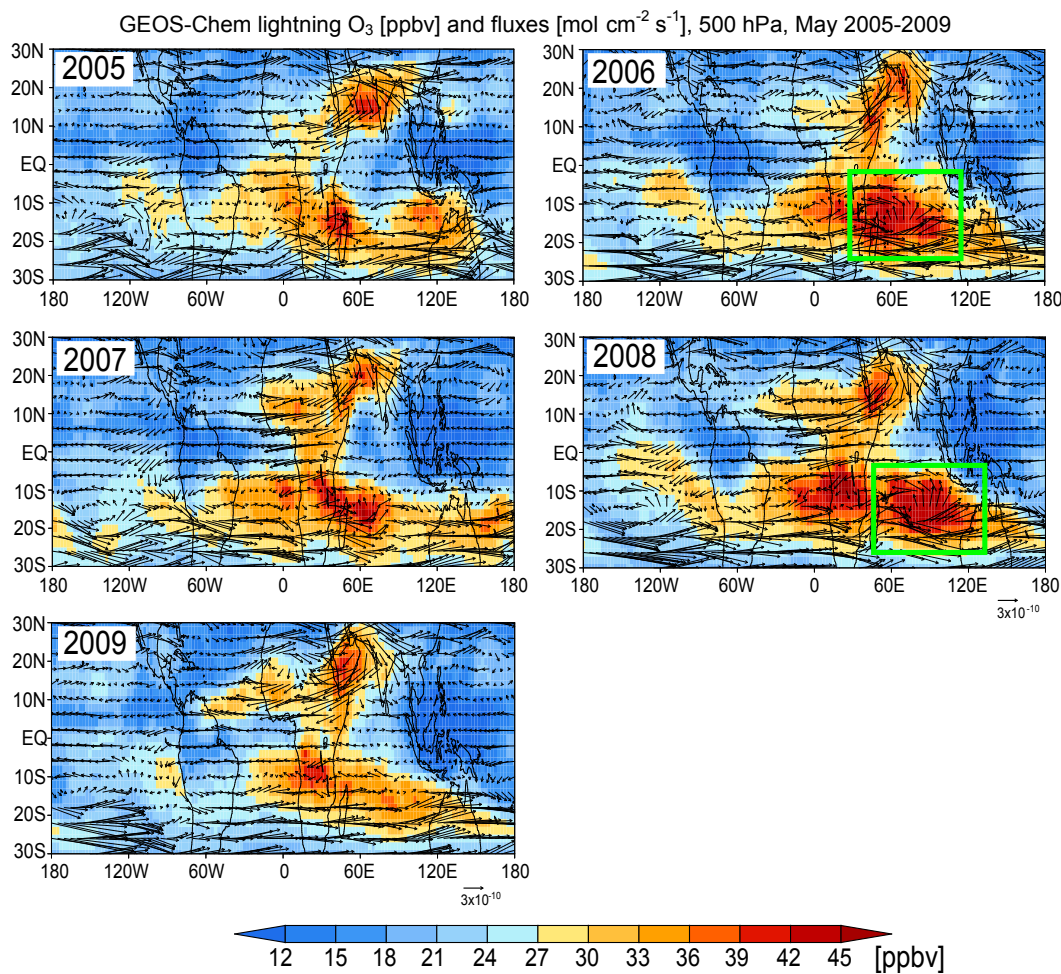


Fig. 17. GEOS-Chem simulated lightning O₃ concentrations (color contours, ppbv) and horizontal fluxes (arrows, mol cm⁻² s⁻¹) at 500 hPa. Lightning O₃ refers to O₃ produced as a result of lightning NO_x emissions. Values are monthly means for May 2005 through 2009. Rectangles indicate regions of anomalous anti-cyclones.

interannual lightning contributions to tropospheric O₃ over the ESIO by turning off lightning NO_x emissions. The results of total and lightning TCO and 215 hPa O₃ are shown in Fig. 15. Lightning NO_x emissions contribute to the peaks of O₃ in May every year from 2005 to 2009 at 215 hPa, which result into the observed O₃ enhancements in the upper tropopause in May 2006 (see Figs. 3, 4, 5, 6 and 13b). The largest contributions to TCO are in 2006 and 2008 (Fig. 15a) and to O₃ (mixing ratios at 215 hPa are shown) in 2005, 2006 and 2008 (Fig. 15b). Lightning O₃ clearly controls the May enhancements. However, there is no apparent interannual variability in the model simulated lightning NO_x emissions from Equatorial Asia, Central Africa and South America – the emissions are not significantly larger in May 2006 and 2008 than in the other three years (Fig. 16). There are clearly additional factors that drive the interannual variability of the tropospheric O₃ maximum in May over the ESIO.

6.3 Anti-cyclonic circulation of Central African and South American lightning outflow

We examine in this section the dynamics as a potential factor for determining the interannual variability of the tropospheric O₃ maximum in May over the ESIO. The lightning O₃ and flux from low troposphere to upper troposphere in May from 2005 to 2009 are investigated. The evident anti-cyclone is only shown in the middle troposphere (500 hPa) over the Southern Indian Ocean in May 2006 and 2008 accompanied with high lightning O₃, even though the lightning O₃ is much higher in the upper troposphere. Fig. 17 shows GEOS-Chem simulated monthly middle tropospheric (500 hPa) lightning O₃ and flux in May for 2005 to 2009. In the Southern Hemisphere, high lightning O₃ are widespread across the southern tropical Indian and South Atlantic Oceans, southern Africa and northern Australia, along the pathways of lightning outflow from Central Africa and South America. The lightning O₃ are much stronger in 2006

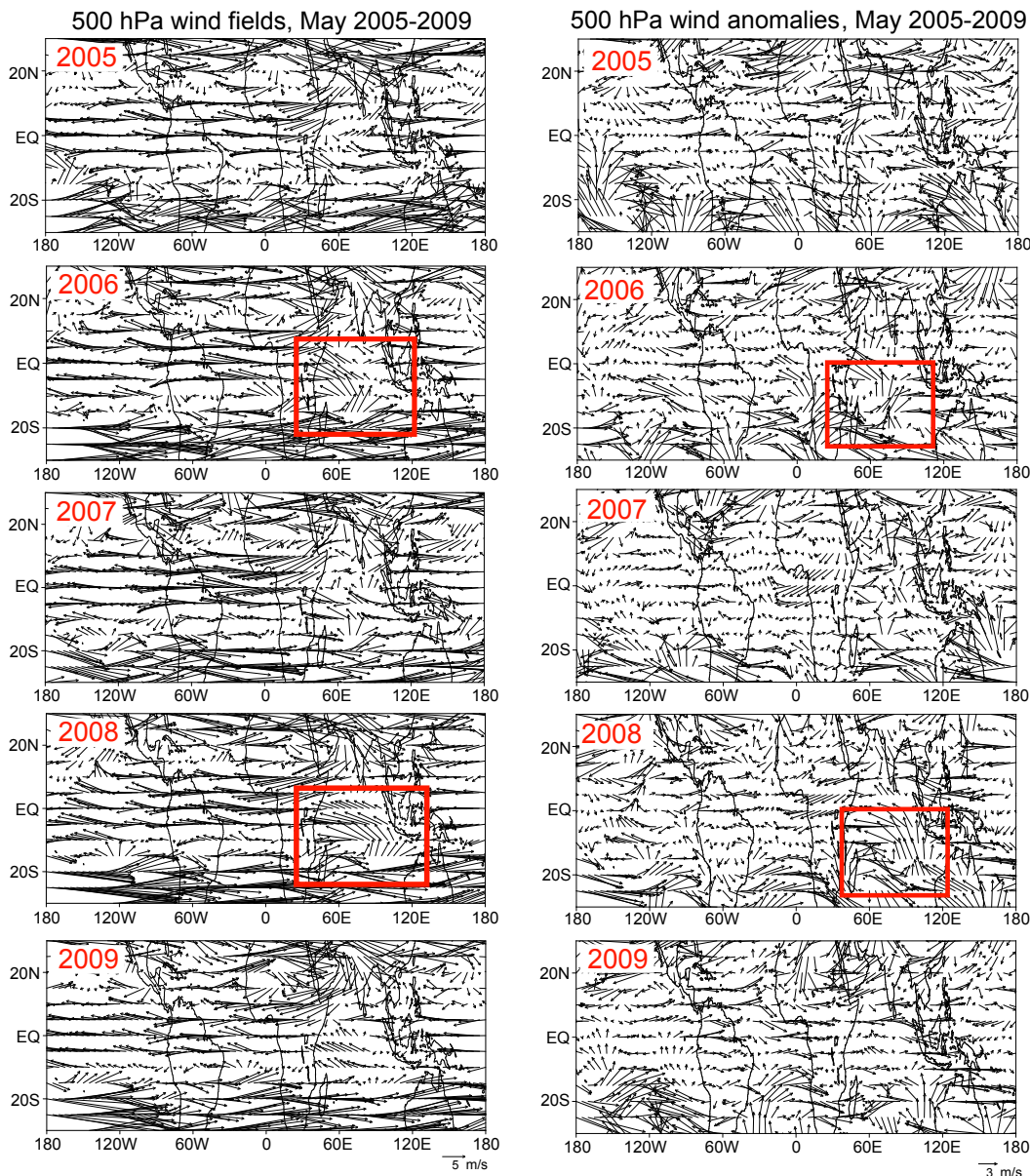


Fig. 18. Monthly mean NCEP wind fields and wind anomalies (m s^{-1}) at 500 hPa for May 2005 through 2009. NCEP reanalysis data provided by the NOAA/OAR/ESRL PSD, Boulder, Colorado, USA, from their web site at <http://www.esrl.noaa.gov/psd/>. Red rectangles indicate regions of anomalous anti-cyclones.

and 2008 than in 2005, 2008 and 2009. There are strong divergences and northward transport of lightning O₃ fluxes over the Southern Indian Ocean in 2006 and 2008. In effect, the anomalous anti-cyclonic circulations in May of 2006 and 2008 effectively entrain and transport O₃ in the African and South American lightning outflow to the ESIO. The divergence and northward transport are largely absent in the other three years. Figure 18 shows the 500 hPa wind fields and the wind anomalies based on 40 years (1970–2009) of climatology from the National Center for Environmental Prediction/National Center for Atmospheric Re-

search (NCEP/NCAR) reanalysis (Kalnay et al., 1996). In May 2006 and 2008, the anti-cyclone circulation and strong northward flows are shown in the wind fields over Southern Indian Ocean, which are less evident in the other years (Fig. 18, left panel). From the anomaly analysis of wind fields, anomalous anti-cyclones and southerly winds are evident in May 2006 and 2008, but not in the other three years (Fig. 18, right panel). Figure 19 shows net O₃ productions at 500 hPa in May. The net O₃ productions are much larger in May 2006 and 2008 than in May 2005, 2007 and 2009. Therefore, the interannual variability of the May O₃

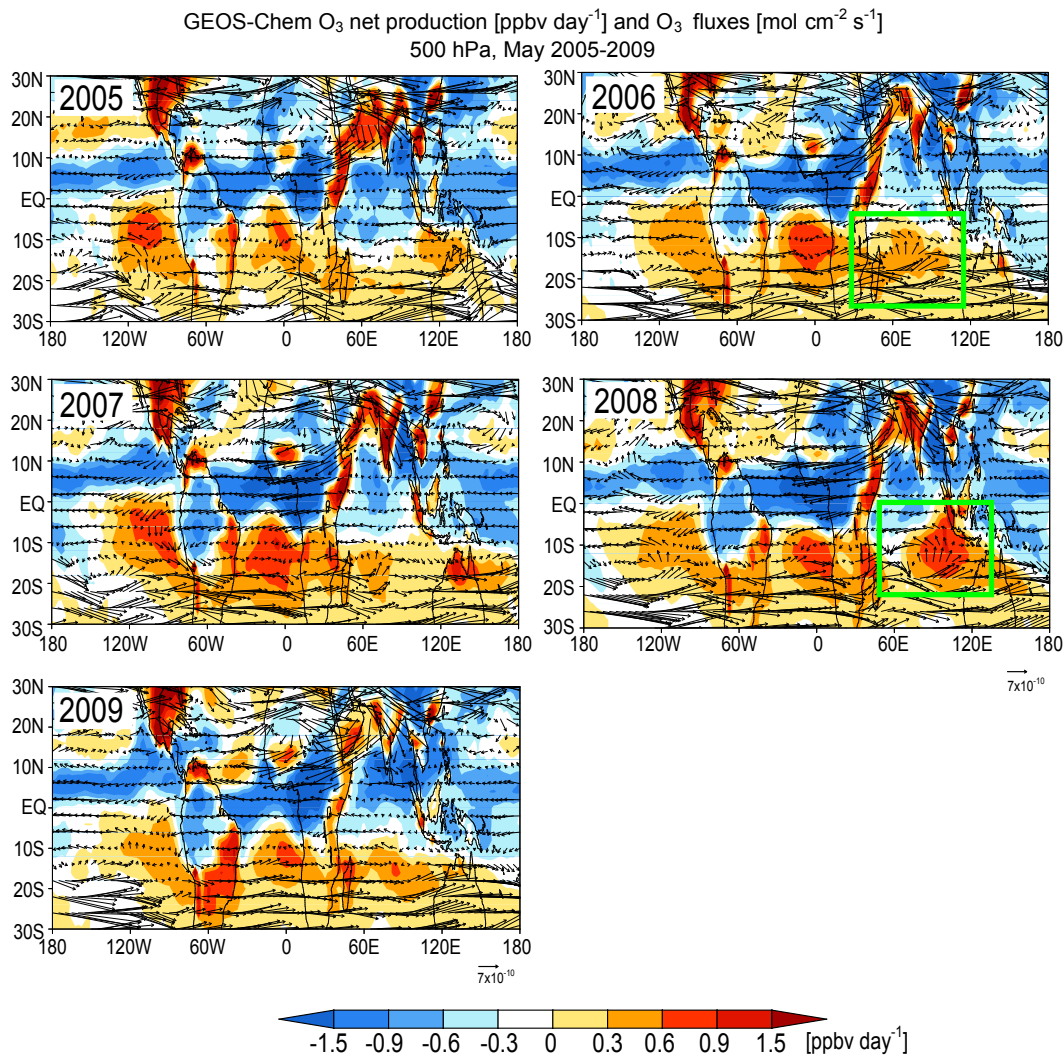


Fig. 19. GEOS-Chem simulated net chemical O_3 production rates (ppbv day^{-1}) and horizontal O_3 fluxes ($\text{mol cm}^{-2} \text{s}^{-1}$) at 500 hPa. Values are monthly means for May 2005 through 2009. Rectangles indicate regions of anomalous anti-cyclones.

maximum in middle troposphere is driven largely by the anomalous anti-cyclones over the southern Indian Ocean in May 2006 and 2008. The lightning NO_x emissions play dominant roles in the upper tropospheric O_3 enhancements (see Figs. 12 and 15b) in May 2005, 2006 and 2008 over the southern Indian Ocean. The combined effect of both lightning and dynamic transport in middle and upper troposphere contributes directly to the interannual variability of TCO, with the evident maximum in May 2006 and 2008.

7 Summary and conclusions

We analyzed 5-year (2005–2009) tropospheric O_3 observations over the Equatorial Southern Indian Ocean (ESIO) from satellite instruments MLS, TES, OMI, and AIRS, using the GEOS-Chem global three-dimensional chemical trans-

port model. Model simulated upper tropospheric O_3 and tropospheric column O_3 (TCO) were compared against the observations. The effects of NO_x sources from lightning, biomass burning, soil, stratospheric downward transport, anthropogenic and biogenic emissions on the tropospheric O_3 over the ESIO, including the seasonal and interannual variability, were examined. In addition, we investigated the effects of dynamics on the interannual variability of tropospheric O_3 over the ESIO.

The satellite observations of tropospheric O_3 showed significant enhancements over the ESIO in May. The enhancements were evident not only in MLS upper tropospheric O_3 , TES middle and upper tropospheric O_3 and TCO, but also in TES, OMI, and AIRS total column O_3 . The enhancements were strongest in 2006 and 2008 and less pronounced in 2005, 2007 and 2009. GEOS-Chem simulations driven by GEOS-5 reanalysis data, with lightning flash rates

parameterized based upon convective cloud top heights, were able to capture the May O₃ enhancements and the associated interannual variability.

We found that lightning contribution accounted for more than 60 % (17 DU) of the total TCO in May 2006, and largely controlled the May O₃ enhancement. The lightning contribution was dominated by lightning NO_x emissions from Equatorial Asia, Central Africa and South America. Equatorial Asian lightning contributed on average ~4 to 5 DU (29.2 % of the total lightning TCO) to the TCO from April through December 2006, with clear enhancements in May 2006. The contributions to the TCO from Central African (~3.5 DU, 20.8 %) and South American (~3.0 DU, 17.9 %) lightning NO_x emissions both showed distinct peaks in May 2006. We found that NO_x emissions from biomass burning, soil, anthropogenic activities and biogenic sources had rather small contributions (less than 2.5 DU) to the tropospheric O₃ enhancements in May 2006. The stratospheric downward transport provided a background about 5 DU throughout the year of 2006.

The larger and more distinct enhancements of TCO in May 2006 and 2008 than those in May 2005, 2007, and 2009 were a directly combined result of the anomalous anti-cyclonic circulations in the middle troposphere and lightning O₃ in the upper troposphere over the Southern Indian Ocean, which were much stronger in 2006 and 2008 than in the other three years. The anomalous anti-cyclonic circulation extended to the middle troposphere. The large-scale subsidence associated with the anti-cyclones served as a conduit that channeled downward the middle and upper tropospheric lightning outflow from Central Africa and South America. As such, lightning O₃ outflows from Central Africa and South America were effectively entrained by the anti-cyclones, followed by northward transport to the ESIO. Therefore, the interannual variability of the tropospheric O₃ enhancements over the ESIO was largely driven by these anomalous anti-cyclones over the Southern Indian Ocean.

Acknowledgements. This research was supported in part by NASA grants NNX09AF07G and NNX08AF64G from the Atmospheric Chemistry Modeling and Analysis Program (ACMAP). We also acknowledge supports by the NASA Aura Science Team program. Work at Jet Propulsion Laboratory, California Institute of Technology was done under contract with the National Aeronautics and Space Administration. The GEOS-Chem model is managed by the Atmospheric Chemistry Modeling group at Harvard University with support from the NASA ACMAP program. We thank Jennifer Logan for helpful discussions.

Edited by: M. Kopacz

References

- Allen, D. J. and Pickering, K. E.: Evaluation of lightning flash rate parameterizations for use in a global chemical transport model, J. Geophys. Res., 107, 4711, doi:10.1029/2002JD002066, 2002.
- Allen, D. J., Kasibhatla, P., Thompson, A. M., Rood, R. B., Doddrige, B. G., Pickering, K. E., Hudson, R. D., and Lin, S.-J.: Transport induced interannual variability of carbon monoxide using a chemistry and transport model, J. Geophys. Res., 101, 28655–28670, 1996a.
- Allen, D. J., Rood, R. B., Thompson, A. M., and Hidson, R. D.: Three-dimensional 222Rn calculations using assimilated data and a convective mixing algorithm, J. Geophys. Res., 101, 6871–6881, 1996b.
- Allen, D. J., Pickering, K. E., Stenchikov, G. L., Thompson, A. M., and Kondo, Y.: A three-dimensional total odd nitrogen (NO_y) simulation during SONEX using a stretched-grid chemical transport model, J. Geophys. Res., 105, 3851–3876, 2000.
- Allen, D. J., Pickering, K. E., Duncan, B., and Damon, M.: Impact of lightning NO emissions on North American photochemistry as determined using the Global Modeling Initiative (GMI) model, J. Geophys. Res., 115, D22301, doi:10.1029/2010JD014062, 2010.
- Aumann, H. H., Chahine, M. T., Gautier, C., Goldberg, M. D., Kalnay, E., McMillin, L. M., Revercomb, H., Rosenkranz, P. W., Smith, W. L., Staelin, D. H., Strow, L. L., and Susskind, J.: AIRS/AMSU/HSB on the Aqua mission: Design, science objectives and data products, IEEE Trans. Geosci. Remote Sens., 41, 253–264, doi:10.1109/TGRS.2002.808356, 2003.
- Balis, D., Kroon, M., Koukouli, M. E., Brinksma, E. J., Labow, G., Veefkind, J. P., and McPeters, R. D.: Validation of Ozone Monitoring Instrument total ozone column measurements using Brewer and Dobson spectrophotometer ground-based observations, J. Geophys. Res., 112, D24S46, doi:10.1029/2007JD008796, 2007.
- Beer, R.: TES on the Aura mission: Scientific objectives, measurements, and analysis overview, IEEE Trans. Geosci. Remote Sens., 44, 1102–1105, doi:10.1109/TGRS.2005.863716, 2006.
- Beer, R., Glavich, T. A., and Rider, D. M.: Tropospheric Emission Spectrometer for the Earth Observing System's Aura satellite, Appl. Optics, 40, 2356–2367, 2001.
- Benkovitz, C., Scholtz, M., Pacyna, J., Tarrasón, L., Dignon, J., Voldner, E., Spiro, P., Logan, J., and Graedel, T.: Global gridded inventories of anthropogenic emissions of sulfur and nitrogen, J. Geophys. Res., 101, 29239–29253, 1996.
- Bey, I., Jacob, D. J., Yantosca, R. M., Logan, J. A., Field, B. D., Fiore, A. M., Li, Q. B., Liu, H. G. Y., Mickley, L. J., and Schultz, M. G.: Global modeling of tropospheric chemistry with assimilated meteorology: Model description and evaluation, J. Geophys. Res., 106, 23073–23096, 2001.
- Bloom, S., Silva, A. da, Dee, D., Bosilovich, M., Chern, J.-D., Pawson, S., Schubert, S., Sienkiewicz, M., Stajner, I., Tan, W.-W., and Wu, M.-L.: Documentation and Validation of the Goddard Earth Observing System (GEOS) Data Assimilation System – Version 4, 2005.
- Bowman, K. W., Rodgers, C. D., Kulawik, S. S., Worden, J., Sarkissian, E., Osterman, G., Steck, T., Luo, M., Eldering, A., Shephard, M., Worden, H., Lampel, M., Clough, S., Brown, P., Rinsland, C., Gunson, M., and Beer, R.: Tropospheric emission spectrometer: Retrieval method and error analysis, IEEE Trans. Geosci. Remote Sens., 44, 1297–1307, doi:10.1109/TGRS.2006.871234, 2006.
- Brasseur, G. P., Hauglustaine, D. A., Walters, S., Rasch, P. J., Müller, J.-F., Granier, C., and Tie, X. X.: MOZART: A global

- chemical transport model for ozone and related chemical tracers: 1. Model description, *J. Geophys. Res.*, 103, 28265–28289, 1998.
- Chandra, S., Ziemke, J. R., Duncan, B. N., Diehl, T. L., Livesey, N. J., and Froidevaux, L.: Effects of the 2006 El Niño on tropospheric ozone and carbon monoxide: implications for dynamics and biomass burning, *Atmos. Chem. Phys.*, 9, 4239–4249, doi:10.5194/acp-9-4239-2009, 2009.
- Chen, Y., Li, Q., Randerson, J. T., Lyons, E. A., Kahn, R. A., Nelson, D. L., and Diner, D. J.: The sensitivity of CO and aerosol transport to the temporal and vertical distribution of North American boreal fire emissions, *Atmos. Chem. Phys.*, 9, 6559–6580, doi:10.5194/acp-9-6559-2009, 2009.
- Christian, H. J., Blakeslee, R. J., Boccippio, D. J., Boeck, W. L., Buechler, D. E., Driscoll, K. T., Goodman, S. J., Hall, J. M., Koshak, W. J., Mach, D. M., and Stewart, M. F.: Global frequency and distribution of lightning as observed from space by the optical transient detector, *J. Geophys. Res.*, 108, 4005, doi:10.1029/2002JD002347, 2003.
- Divakarla, M., Barnet, C., Goldberg, M., Maddy, E., Irion, F., Newchurch, M., Liu, X. P., Wolf, W., Flynn, L., Labow, G., Xiong, X. Z., Wei, J., and Zhou, L.: Evaluation of Atmospheric Infrared Sounder ozone profiles and total ozone retrievals with matched ozonesonde measurements, ECMWF ozone data, and Ozone Monitoring Instrument retrievals, *J. Geophys. Res.*, 113, D15308, doi:10.1029/2007JD009317, 2008.
- Fishman, J., Watson, C. E., Larsen, J. C., and Logan, J. A.: Distribution of tropospheric ozone determined from satellite data, *J. Geophys. Res.*, 95, 3599–3617, 1990.
- Giglio, L., Descloitres, J., Justice, C. O., and Kaufman, Y. J.: An enhanced contextual fire detection algorithm for MODIS. *Remote Sensing of Environment*, 87, 273–282, 2003.
- Giglio, L., van der Werf, G. R., Randerson, J. T., Collatz, G. J., and Kasibhatla, P.: Global estimation of burned area using MODIS active fire observations, *Atmos. Chem. Phys.*, 6, 957–974, doi:10.5194/acp-6-957-2006, 2006.
- Guenther, A., Karl, T., Harley, P., Wiedinmyer, C., Palmer, P. I., and Geron, C.: Estimates of global terrestrial isoprene emissions using MEGAN (Model of Emissions of Gases and Aerosols from Nature), *Atmos. Chem. Phys.*, 6, 3181–3210, doi:10.5194/acp-6-3181-2006, 2006.
- Hack, J. J.: Parameterization of moist convection in the NCAR community climate model (CCM2), *J. Geophys. Res.*, 99, 5551–5568, doi:10.1029/93JD03478, 1994.
- Horowitz, L., Walters, S., Mauzerall, D., Emmons, L., Rasch, P., Granier, C., Tie, X., Lamarque, J.-F., Schultz, M., Tindall, G., Orlando, J., and Brasseur, G.: A global simulation of tropospheric ozone and related tracers: Description and evaluation of MOZART, version 2, *J. Geophys. Res.*, 108, 4784, doi:10.1029/2002JD002853, 2003.
- Hudman, R. C., Jacob, D. J., Turquety, S., Leibensperger, E. M., Murray, L. T., Wu, S., Gilliland, A. B., Avery, M., Bertram, T. H., Brune, W., Cohen, R. C., Dibb, J. E., Flocke, F. M., Fried, A., Holloway, J., Neuman, J. A., Orville, R., Perring, A., Ren, X., Sachse, G. W., Singh, H. B., Swanson, A., and Wooldridge, P. J.: Surface and lightning sources of nitrogen oxides over the United States: Magnitudes, chemical evolution, and outflow, *J. Geophys. Res.*, 112, D12S05, doi:10.1029/2006JD007912, 2007.
- Jacob, D. J., Heikes, B. G., Fan, S.-M., Logan, J. A., Mauzerall, D. L., Bradshaw, J. D., Singh, H. B., Gregory, G. L., Talbot, R. W., Blake, D. R., and Sachse, G. W.: Origin of ozone and NO_x in the tropical troposphere: a photochemical analysis of aircraft observations over the South Atlantic Basin, *J. Geophys. Res.*, 101, 24235–24350, 1996.
- Jourdain, L., Worden, H. M., Bowman, K., Li, Q. B., Eldering, A., Kulawik, S. S., Osterman, G., Boersma, K. F., Fisher, B., Rinsland, C. P., Beer, R., and Gunson, M.: Tropospheric vertical distribution of tropical Atlantic ozone observed by TES during the northern African biomass burning season, *Geophys. Res. Lett.*, 34, L04810, doi:10.1029/2006GL028284, 2007.
- Jourdain, L., Kulawik, S. S., Worden, H. M., Pickering, K. E., Worden, J., and Thompson, A. M.: Lightning NO_x emissions over the USA constrained by TES ozone observations and the GEOS-Chem model, *Atmos. Chem. Phys.*, 10, 107–119, doi:10.5194/acp-10-107-2010, 2010.
- Kalnay, E., Kanamitsu, M., Kistler, R., Collins, W., Deaven, D., Gandin, L., Iredell, M., Saha, S., White, G., Woollen, J., Zhu, Y., Leetmaa, A., Reynolds, B., Chelliah, M., Ebisuzaki, W., Higgins, W., Janowiak, J., Mo, K.C., Ropelewski, C., Wang, J., Jenne, R., and Joseph, D.: The NCEP/NCAR 40-year reanalysis project, *B. Am. Meteorol. Soc.*, 77, 437–471, 1996.
- Komala, N., Saraswati, S., Kita, K., and Ogawa, T.: Tropospheric ozone behavior observed in Indonesia, *Atmos. Environ.*, 30, 1851–1856, 1996.
- Kulawik, S. S., Worden, J., Eldering, A., Bowman, K., Gunson, M., Osterman, G. B., Zhang, L., Clough, S., Shephard, M. W., and Beer, R.: Implementation of cloud retrievals for Tropospheric Emission Spectrometer (TES) atmospheric retrievals: part 1. Description and characterization of errors on trace gas retrievals, *J. Geophys. Res.*, 111, D24204, doi:10.1029/2005JD006733, 2006.
- Lacis, A. A., Wuebbles, D. J., and Logan, J. A.: Radiative forcing of climate by changes in the vertical distribution of ozone, *J. Geophys. Res.*, 95, 9971–9981, doi:10.1029/JD095iD07p09971, 1990.
- Leveld, P. F., Hilsenrath, E., Leppelmeier, G. W., van den Oord, G. H. J., Bhartia, P. K., Tamminen, J., de Haan, J. F., and Veefkind, J. P.: Science objectives of the Ozone Monitoring Instrument, *IEEE Trans. Geosci. Remote Sens.*, 44, 1199–1208, doi:10.1109/TGRS.2006.872336, 2006a.
- Leveld, P. F., van den Oord, G. H. J., Dobber, M. R., Mälkki, A., Visser, H., de Vries, J., Stammes, P., Lundell, J. O. V., and Saari, H.: The Ozone Monitoring Instrument, *IEEE Trans. Geosci. Remote Sens.*, 44, 1093–1101, doi:10.1109/TGRS.2006.872333, 2006b.
- Levy, H.: Normal atmosphere: Large radical and formaldehyde concentrations predicted, *Science*, 173, 141–143, 1971.
- Lin, S. J. and Rood, R. B.: Multidimensional flux form semi-Lagrangian transport schemes, *Mon. Weather Rev.*, 124, 2046–2070, 1996.
- Liu, J. J., Jones, D. B. A., Worden, J. R., Noone, D., Parrington, M., and Kar, J.: Analysis of the summertime buildup of tropospheric ozone abundances over the Middle East and North Africa as observed by the Tropospheric Emission Spectrometer instrument, *J. Geophys. Res.*, 114, D05304, doi:10.1029/2008JD010993, 2009.
- Liu, J. J., Jones, D. B. A., Zhang, S., and Kar, J.: Influence of interannual variations in transport on summertime abundances of ozone over the Middle East, *J. Geophys. Res.*, 116, D20310,

- doi:10.1029/2011JD016188, 2011.
- Livesey, N. J., Snyder, W. V., Read, W. G., and Wagner, P. A.: Retrieval algorithms for the EOS Microwave Limb Sounder (MLS) instrument, *IEEE Trans. Geosci. Remote Sens.*, 44, 1144–1155, 2006.
- Livesey, N. J., Filipiak, M., Froidevaux, L., Read, W., Lambert, A., Santee, M., Jiang, J., Waters, J., Drouin, B., Cofield, R., Cuddy, D., Fuller, R., Jarnot, R., Jiang, Y., Knosp, B., Li, Q. B., Schwartz, M., Snyder, W., Stek, P., Wagner, P., Pumphrey, H., Avery, M., Browell, E., Christensen, L., Edwards, D., Emmons, L., Fahey, D., Gao, R., Loewenstein, M., Lopez, J., Osterman, G., Sachse, G., and Webster, C.: Validation of EOS MLS O₃ and CO observations in the upper troposphere and lower stratosphere, *J. Geophys. Res.*, 113, D15S02, doi:10.1029/2007JD008805, 2008.
- Livesey, N. J., Read, G. W., Froidevaux, L., Lambert, A., Manney, L. G., Pumphrey, C. H., Santee, L. M., Schwartz, J. M., Wang, S., Cofield, E. R., Cuddy, T. D., Fuller A. R., Jarnot, F. R., Jiang, H. J., Knosp, W. B., Stek C. P., Wagner, A. P., and Wu, L. D.: Version 3.3 Level 2 data quality and description document, Jet Propulsion Laboratory, 2011.
- Logan, J. A., Prather, M. J., Wofsy, S. C., and McElroy, M. B.: Tropospheric chemistry: A global perspective, *J. Geophys. Res.*, 86, 7210–7254, 1981.
- Logan, J. A., Megretskaya, I., Nassar, R., Murray, T. L., Zhang, L., Bowman, W. K., Worden, W. H., and Luo, M.: Effects of the 2006 El Niño on tropospheric composition as revealed by data from the Tropospheric Emission Spectrometer (TES), *Geophys. Res. Lett.*, 35, L03816, doi:10.1029/2007GL031698, 2008.
- Luo, M., Rinsland, C. P., Logan, J. A., Worden, J., Kulawik, S., Eldering, A., Goldman, A., Shephard, M. W., Gunson, M., and Lampel M.: Comparison of carbon monoxide measurements by TES and MOPITT: The influence of a priori data and instrument characteristics on nadir atmospheric species retrievals, *J. Geophys. Res.*, 112, D09303, doi:10.1029/2006JD007663, 2007.
- Martin, R. V., Sauvage, B., Folkins, I., Sioris, C. E., Boone, C., Bernath, P., and Ziemke, J.: Space-based constraints on the production of nitric oxide by lightning, *J. Geophys. Res.*, 112, D09309, doi:10.1029/2006JD007831, 2007.
- McLinden, C. A., Olsen, S. C., Hannegan, B., Wild, O., Prather, M. J., and Sundet, J.: Stratospheric ozone in 3-D models: A simple chemistry and the cross-tropopause flux, *J. Geophys. Res.*, 105, 14653–14666, 2000.
- McPeters, R., Kroon, M., Labow, G., Brinksma, E., Balis, D., Petropavlovskikh, I., Veefkind, J. P., Bhartia, P. K., and Levitt, P. F.: Validation of the Aura Ozone Monitoring Instrument total column ozone product, *J. Geophys. Res.*, 113, D15S14, doi:10.1029/2007JD008802, 2008.
- Moorthi, S. and Suarez, M. J.: Relaxed Arakawa–Schubert: A parameterization of moist convection for general circulation models, *Mon. Weather Rev.*, 120, 978–1002, 1992.
- Murray, L. T., Jacob, D. J., Logan, J. A., Hudman, R. C., and Koshak, W. J.: Optimized regional and interannual variability of lightning in a global chemical transport model constrained by LIS/OTD satellite data, *J. Geophys. Res.*, submitted, 2012.
- Nassar, R., Logan, J. A., Worden, H. M., Megretskaya, I. A., Bowman, K. W., Osterman, G. B., Thompson, A. M., Tarasick, D. W., Austin S., Claude, H., Dubey, M. K., Hocking, W. K., Johnson, B. J., Joseph, E., Merrill, J., Morris, G. A., Newchurch, M., Oltmans, S. J., Posny, F., Schmidlin, F. J., Vomel, H., Whiteman, D. N., and Witte, J. C.: Validation of Tropospheric Emission Spectrometer (TES) nadir ozone profiles using ozonesonde measurements, *J. Geophys. Res.*, 113, D15S17, doi:10.1029/2007JD008819, 2008.
- Nassar, R., Logan, J. A., Megretskaya, I. A., Murray, L. T., Zhang, L., and Jones, D. B. A.: Analysis of tropospheric ozone, carbon monoxide and water vapor during the 2006 El Niño using TES observations and the GEOS-Chem model, *J. Geophys. Res.*, 114, D17304, doi:10.1029/2009JD011760, 2009.
- Olivier, J. G. J. and Berdowski, J. J. M.: Global emissions sources and sinks, in: *The Climate System*, edited by: Berdowski, J., Guicherit, R., and Heij, B. J., pp. 33–78, A. A. Balkema, Lisse, Netherlands, 2001.
- Oman, L. D., Ziemke, J. R., Douglass, A. R., Waugh, D. W., Lang, C., Rodriguez, J. M., and Nielsen, J. E.: The response of tropical tropospheric ozone to ENSO, *Geophys. Res. Lett.*, 38, L13706, doi:10.1029/2011GL047865, 2011.
- Osterman, G. B., Kulawik, S. S., Worden, H., Richards, N. A., Fisher, B. M., Eldering, A., Shephard, M. W., Froidevaux, L., Labow, G., Luo, M., Herman, R. L., Bowman, K. W., and Thompson, A. M.: Validation of Tropospheric Emission Spectrometer (TES) measurements of the total, stratospheric, and tropospheric column abundance of ozone, *J. Geophys. Res.*, 113, D15S16, doi:10.1029/2007JD008801, 2008.
- Parkinson, C. L.: Aqua: An Earth-observing satellite mission to examine water and other climate variables, *IEEE Transactions on Geoscience and Remote Sensing*, 41, 173–183, doi:10.1109/TGRS.2002.808319, 2003.
- Pickering, K. E., Wang, Y. S., Tao, W. K., Price, C., and Muller, J. F.: Vertical distributions of lightning NO_x for use in regional and global chemical transport models, *J. Geophys. Res.*, 103, 31203–31216, 1998.
- Price, C. and Rind, D. H.: A simple lightning parameterization for calculating global lightning distributions, *J. Geophys. Res.*, 97, 9919–9933, 1992.
- Price, C. and Rind, D. H.: What determines the cloud-to-ground lightning fraction in thunderstorms?, *Geophys. Res. Lett.*, 20, 463–466, 1993.
- Price, C. and Rind, D. H.: Modeling global lightning distributions in a general circulation model, *Mon. Weather Rev.*, 122, 1930–1939, 1994.
- Randerson, J. T., Liu, H., Flanner, M. G., Chambers, S. D., Jin, Y., Hess, P. G., Pfister, G., Mack, M. C., Treseder, K. K., Welp, L. R., Chapin, F. S., Harden, J. W., Goulden, M. L., Lyons, E., Neff, J. C., Schuur, E., and Zender, C. S.: The impact of boreal forest fire on climate warming, *Science*, 314, 1130–1132, 2006.
- Rienecker, M.: File specification for GEOS-5 DAS gridded output, NASA Goddard Space Flight Center, 2008.
- Sander, S. P., Friedl, R. R., DeMore, W. B., Golden, D. M., Kurylo, M. J., Hampson, R. F., Huie, R. E., Moortgat, G. K., Ravishankara, A. R., Kolb, C. E., and Molina, M. J.: Chemical Kinetics and Photochemical Data for Use in Stratospheric Modeling, Technical Report JPL Publication 00-3, Jet Propulsion Laboratory, Pasadena, CA, 2000.
- Sauvage, B., Martin, R. V., van Donkelaar, A., Liu, X., Chance, K., Jaeglé, L., Palmer, P. I., Wu, S., and Fu, T.-M.: Remote sensed and in situ constraints on processes affecting tropical tropospheric ozone, *Atmos. Chem. Phys.*, 7, 815–838, doi:10.5194/acp-7-815-2007, 2007.

- Schoeberl, M. R., Douglass, A. R., Hilsenrath, E., Bhartia, P. K., Beer, R., Waters, J. W., Gunson, M. R., Froidevaux, L., Gille, J. C., Barnett, J. J., Levelt, P. F., and DeCola, P.: Overview of the EOS Aura mission, *IEEE Trans. Geosci. Remote Sens.*, 44, 1066–1074, doi:10.1109/TGRS.2005.861950, 2006.
- Shim, C., Li, Q. B., Luo, M., Kulawik, S., Worden, H., Worden, J., Eldering, A., Avery, M., Diskin, G., Sachse, G.: A Weinheimer, D. Knapp, D. Montzca, and T. Campos, Satellite observations of Mexico City pollution outflow from the Tropospheric Emissions Spectrometer (TES), *Atmos. Environ.*, 43, 1540–1547, doi:10.1016/j.atmosenv.2008.11.026, 2009.
- Tan, W., Geller, M. A., Pawson, S., and da Silva, A. M.: A case study of excessive subtropical transport in the stratosphere of a data assimilation system, *J. Geophys. Res.*, 109, D11102, doi:10.1029/2003JD004057, 2004.
- Thompson, A. M., Pickering, K. E., McNamara, D. P., Schoeberl, M. R., Hudson, R. D., Kim, J. H., Browell, E. V., Kirchhoff, V. W. J. H., and Nganga, D.: Where did tropospheric ozone over southern Africa and the tropical Atlantic come from in October 1992? Insights from TOMS, GTE TRACE-A and SAFARI 1992, *J. Geophys. Res.*, 101, 24251–24278, doi:10.1029/96JD01463, 1996.
- Thompson, A. M., Witte, J. C., Hudson, R. D., Guo, H., Herman, J. R., and Fujiwara, M.: Tropical tropospheric ozone and biomass burning, *Science*, 291, 2128–2132, doi:10.1126/science.291.5511.2128, 2001.
- van der Werf, G. R., Randerson, J. T., Giglio, L., Collatz, G. J., Kasibhatla, P. S., and Arellano Jr., A. F.: Interannual variability in global biomass burning emissions from 1997 to 2004, *Atmos. Chem. Phys.*, 6, 3423–3441, doi:10.5194/acp-6-3423-2006, 2006.
- Wang, Y., Jacob, D. J., and Logan, J. A.: Global simulation of tropospheric O₃-NO_x-hydrocarbon chemistry. 1. Model formulation, *J. Geophys. Res.*, 103, 10713–10726, 1998.
- Waters, J. W., Froidevaux, L., Harwood, R. S., Jarnot, R. F., Pickett, H. M., Read, W. G., Siegel, P. H., Cofield, R. E., Filipiak, M. J., Flower, D. A., Holden, J. R., Lau, G. K., Livesey, N. J., Manney, G. L., Pumphrey, H. C., Santee, M. L., Wu, D. L., Cuddy, D. T., Lay, R. R., Loo, M. S., Perun, V. S., Schwartz, M. J., Stek, P. C., Thurstans, R. P., Boyles, M. A., Chandra, K. M., Chavez, M. C., Chen, G. S., Chudasama, B. V., Dodge, R., Fuller, R. A., Girard, M. A., Jiang, J. H., Jiang, Y., Knosp, B. W., LaBelle, R. C., Lam, J. C., Lee, K. A., Miller, D., Oswald, J. E., Patel, N. C., Pukala, D. M., Quintero, O., Scaff, D. M., Van Snyder, W., Tope, M. C., Wagner, P. A., and Walch, M. J.: The Earth Observing System Microwave Limb Sounder (EOS MLS) on the Aura satellite, *IEEE Trans. Geosci. Remote Sens.*, 44, 1075–1092, doi:10.1109/TGRS.2006.873771, 2006.
- Weaver, C. J., Douglass, A. R., and Rood, R. B.: Thermodynamic balance of three-dimensional stratospheric winds derived from a data assimilation procedure, *J. Atmos. Sci.*, 50, 2987–2993, 1993.
- Wild, O., Zhu, X., and Prather, M. J.: FAST-J: Accurate simulation of in- and below-cloud photolysis in tropospheric chemical models, *J. Atmos. Chem.*, 37, 245–282, 2000.
- Worden, H. M., Logan, J. A., Worden, J. R., Beer, R., Bowman, K., Clough, S. A., Eldering, A., Fisher, B. M., Gunson, M. R., Herman, R. L., Kulawik, S. S., Lampel, M. C., Luo, M., Meqretskaya, I. A., Osterman, G. B., and Shephard, M. W.: Comparisons of Tropospheric Emission Spectrometer (TES) ozone profiles to ozonesondes: Methods and initial results, *J. Geophys. Res.*, 112, D03309, doi:10.1029/2006JD007258, 2007.
- Yevich, R. and Logan, J. A.: An assessment of biofuel use and burning of agricultural waste in the developing world, *Global Biogeochem. Cycles*, 17, 1095, doi:10.1029/2002GB001952, 2003.
- Zhang, G. J. and McFarlane, N. A.: Sensitivity of climate simulations to the parameterization of cumulus convection in the Canadian climate centre general circulation model, *Atmos.-Ocean*, 33, 407–446, 1995.
- Zhang, Q., Streets, D. G., Carmichael, G. R., He, K. B., Huo, H., Kannari, A., Klimont, Z., Park, I. S., Reddy, S., Fu, J. S., Chen, D., Duan, L., Lei, Y., Wang, L. T., and Yao, Z. L.: Asian emissions in 2006 for the NASA INTEX-B mission, *Atmos. Chem. Phys.*, 9, 5131–5153, doi:10.5194/acp-9-5131-2009, 2009.
- Zhang, L., Li, Q. B., Jin, J., Liu, H., Livesey, N., Jiang, J. H., Mao, Y., Chen, D., Luo, M., and Chen, Y.: Impacts of 2006 Indonesian fires and dynamics on tropical upper tropospheric carbon monoxide and ozone, *Atmos. Chem. Phys.*, 11, 10929–10946, doi:10.5194/acp-11-10929-2011, 2011.
- Ziemke, J. R., Chandra, S., Duncan, B. N., Schoeberl, M. R., Torres, O., Damon, M. R., and Bhartia, P. K.: Recent biomass burning in the tropics and related changes in tropospheric ozone, *Geophys. Res. Lett.*, 36, L15819, doi:10.1029/2009GL039303, 2009.